Journal of Geochemical Exploration 249 (2023) 107214

Contents lists available at ScienceDirect

Journal of Geochemical Exploration

journal homepage: www.elsevier.com/locate/gexplo

A conceptual model for the Tufiño-Chiles-Cerro Negro (TCCN) geothermal system (Ecuador-Colombia): New insights into geothermal exploration from chemical and isotopic composition of hydrothermal fluids

Marco Taussi [a], Daniele Tardani [b,c,*], Franco Tassi [d], Andrea Gorini [a], Eduardo Aguilera [e], Bruno Capaccioni [f,1], Alberto Renzulli [a]

[a] University of Urbino Carlo Bo, Department of Pure and Applied Sciences, Urbino, Italy
[b] University of O'Higgins, Institute of Engineering Sciences, Rancagua, Chile
[c] Andean Geothermal Centre of Excellence (CEGA), University of Chile, Santiago, Chile
[d] University of Florence, Department of Earth Sciences, Firenze, Italy
[e] Universidad de la Fuerzas Armadas (ESPE), Sangolquí, Ecuador
[f] University of Bologna Alma Mater Studiorum, Department of Biological, Geological and Environmental Sciences, Bologna, Italy

ARTICLE INFO

Keywords:
Tufiño-Chiles-Cerro Negro
Geothermal system
Fluid geochemistry
Stable isotopes
Andean Northern Volcanic Zone
Gas geothermometry

ABSTRACT

The Tufiño-Chiles-Cerro Negro (TCCN), located on the border between Colombia and Ecuador, is one of the most promising geothermal systems in the Andean Northern Volcanic Zone, presenting an estimated geothermal potential of 130–138 MWe associated with two reservoirs located at 500–1000 m, and > 1500 m of depth, respectively. In this work, we present a geochemical conceptual model for TCCN to explore the physicochemical conditions acting on the reservoir, based on a comprehensive dataset of water, gas geochemistry, and stable isotopes of the hydrothermal manifestations of the geothermal system, integrated with previously published data. Four new water samples and two bubbling gas samples were collected from the TCCN area during fieldwork in January 2015. Waters from TCCN, which show temperatures up to 54.7 °C, are near-neutral to slightly acidic and have variable TDS values (687 to 3095 mg/L) that generally increase at increasing temperature. All the samples fall far from the chloride-mature waters field, being characterised by SO_4^{2-} or HCO_3^--dominated composition, suggesting steam-heated and peripheral water characteristics. The $^3He/^4He$ ratios (R/Ra) of gas samples range between 2.4 and 4.6, indicating an important mantle He contribution diluted by the addition of radiogenic and atmospheric ^4He. Based on their $CO_2/^3He$ and $\delta^{13}C–CO_2$ ratios, gas samples show a carbon origin prevailing from subducted limestone, likely connected to the presence of the subducting Carnegie ridge. A mixing between a thermogenic and biogenic origin for methane is suggested, consistent with the dominant inputs from microbial methanogenesis and thermal maturation of sedimentary organic matter in the TCCN system. The high $\delta^{34}S$-H_2S values of gas (+6.7 ‰ and 10.7 ‰ vs. V-CDT) and $\delta^{34}S$-SO_4 of water (+19.2 ‰ and + 19.3 ‰ vs. V-CDT) samples coupled with the high values of $S/^3He$ indicate that the sulphur signature could be mostly controlled by the incorporation of subducted sulphate. Gas geothermometric estimations in the CO_2-H_2 system indicate a temperature between 245 and 250 °C for the geothermal reservoir. The gas samples appear to be in disequilibrium concerning the redox conditions related to the FeO/FeO1.5 buffer typical for hydrothermal systems, implying that these samples represent immature vapours. This could be explained by the input of magmatic fluids into the roots of the TCCN geothermal systems, possibly related to the seismic crisis linked to the unrest of the volcanic complex at the end of 2014.

* Corresponding author at: Institute of Engineering Science, O'Higgins University, Av. Libertador Bernardo O'Higgins 611, Rancagua, Chile.
E-mail address: daniele.tardani@uoh.cl (D. Tardani).
[1] Deceased

https://doi.org/10.1016/j.gexplo.2023.107214
Received 3 August 2022; Received in revised form 31 January 2023; Accepted 27 March 2023
Available online 31 March 2023

1. Introduction

Geothermal activity in northern Ecuador and Colombia is closely associated with the Late-Pliocene to present-day volcanism (Hall et al., 2008; Inguaggiato et al., 2010; Mejía et al., 2014) of the Andean Northern Volcanic Zone (Fig. 1a), which comprises large stratovolcanoes, caldera complexes and lava domes (Hall et al., 2008). The gross geothermal-electric potential of Ecuador was estimated at 500–3000 MWe (Bona and Coviello, 2016 and references therein), while that of Colombia at 700–1370 MWe (Alfaro et al., 2021; Gawell et al., 1999). Despite this enormous, estimated potential and the presence of numerous hydrothermal systems along the arc (Almeida et al., 1992; Gómez and Marín Cerón, 2020; Inguaggiato et al., 2010; Taborda et al., 2022), the signs of progress of the various geothermal projects of the two countries still do not go beyond the exploratory phase (Alfaro and Rodriguez, 2021; Beate et al., 2021; Salazar et al., 2017). In fact, to date, the only two deep exploration wells in Ecuador and Colombia were drilled at the Chachimbiro (Ecuador; Beate et al., 2021) and Nevado del Ruiz geothermal systems (Colombia; Vélez et al., 2018). As a matter of fact, the only geothermal power plant in South America is still represented by the Cerro Pabellón project in Chile (Maza et al., 2021).

The Tufiño-Chiles-Cerro Negro (TCCN) geothermal system, which is located on the border between Colombia and Ecuador, 25 km W of Tulcán (Ecuador) and 20 km SW of Cumbal (Colombia) (Fig. 1b), is one of the most promising geothermal areas in the Northern Andes. In this area, preliminary geochemical and geophysical prospecting have been carried out since the '80s, in the framework of a collaboration of Colombian and Ecuadorian institutes such as ICEL (Colombia) and INECEL (Ecuador) with the support of Aquater Ltd. (Italy). Based on the results of these studies, a geothermal potential of 130–138 MWe was estimated (Bona and Coviello, 2016; Mejía et al., 2014), likely associated with two reservoirs located at different depths (i.e., 500–1000 m, and > 1500 m of depth, respectively; Bona and Coviello, 2016 and references therein; Coviello, 2000; Garcia and Sanchez, 2019; INECEL-OLADE-AQUATER, 1987). Although these studies represent a noteworthy step forward in the knowledge of TCCN, the available data for this geothermal system are not coherently presented and interpreted yet.

In this work, we present a conceptual model for TCCN based on a comprehensive dataset of water and gas geochemistry and stable isotopes on the hydrothermal manifestations of the geothermal system. Our data were integrated with those previously published (Fig. 1c; Carrera and Guevare, 2016; Inguaggiato et al., 2010;) and those available from the National Inventory of Hydrothermal Manifestations of the Colombia Geological Survey (SGC, 2020). The main aim of the present contribution is thus to present a comprehensive geochemical conceptual model to describe the physicochemical conditions acting on the fluid reservoir and to define the processes controlling fluid chemistry.

2. General background

2.1. Geological setting

The Quaternary volcanic arcs of Ecuador and Colombia are the result of the eastward subduction of the Miocene Nazca oceanic Plate (<25 Ma; Barckhausen et al., 2008; Müller et al., 2008; Seton et al., 2012) beneath the South American Plate. The subducting plate carries an aseismic volcanic plateau, namely the Carnegie Ridge (Fig. 1b), formed by the eastward motion of the Nazca Plate over the Galapagos hotspot (Michaud et al., 2009 and references therein). The volcanic features are distributed, from West to East, in the Western Cordillera (frontal arc), the Inter-Andean Depression and Eastern Cordillera (main arc), and the Sub-Andean Zone (back-arc region) (Ancellin et al., 2017; Bryant et al., 2006; Hall and Beate, 1991; Hall et al., 2008; Hidalgo et al., 2012;). The continental arc consists of >70 volcanoes (Stern, 2004), of which at least 20 have been active in the Holocene (Hall et al., 2008). Among these volcanoes, Chiles and Cerro Negro (Fig. 1c) are two adjacent potentially active stratovolcanoes (www.igepn.edu.ec; Cortés and Calvache, 1996) with an elevation of 4698 and 4445 m a.s.l. respectively. Due to their proximity, they are considered to be fed by the same magmatic system (INECEL-OLADE-AQUATER, 1987). They are part of the northern sector of the Western Cordillera (Ancellin et al., 2017; Droux and Delaloye, 1996) and lie at the border between the province of Carchi (Ecuador) and the department of Nariño (Colombia), about 7 km West of the villages of Tufiño (Ecuador) and Chiles (Colombia) (Fig. 1b). The most significant morphological features are horseshoe-shaped collapsing structures affecting the northern slope of Chiles and the western slope of Cerro Negro, respectively (Fig. 1c), and landscape forms linked to glacial moraine deposits (Cortés and Calvache, 1996; Garcia and Sanchez, 2019).

The volcanoes were built upon the top of a thick sequence of Pliocene andesitic lavas (4.8 Ma; ICEL, 1983) overlying volcano-sedimentary deposits of the Nariño Formation and accreted oceanic crust of Cretaceous age (Pallatanga Terrain), with an associated island arc (Río Cala Formation) and trench sediments (Natividad Formation) of Mid-Late Cretaceous age (Beate and Urquizo, 2015). Lavas of both volcanoes are mainly medium-K calc-alkaline andesites and dacites (Droux and Delaloye, 1996). Chiles volcano activity was mostly effusive and produced thick lava flows (Cortés and Calvache, 1996) between 500 and 5 ka (INECEL-OLADE-AQUATER, 1987). Cerro Negro consists of two superimposed structures with the oldest one dated at ~1.4 Ma and the youngest at 40 ka (INECEL-OLADE-AQUATER, 1987). Its products comprise both lavas and pyroclastics (including ignimbrite) and debris avalanches associated with the collapse of the flank (Cortés and Calvache, 1996).

The analysis of records of the volcanic activity suggests that these volcanoes had minor eruptive events in historical periods (Monsalve, 2020; Monsalve and Laverde, 2016), although Santamaria et al. (2017) ruled out any possible explosive activity related to the Cerro Negro or Chiles volcanoes in the last ~7 ka. Since the end of 2013 and up to the end of 2014, three seismic swarms have been detected about 2–6 km South of Chiles Volcano (Ebmeier et al., 2016). All the seismic sequences occurred, mainly, in the same location and most of the earthquakes had depths between 2 and 5 km, with magnitude <4, concentrated in an area of ~25 km^2. These earthquakes have been related to volcano-tectonic seismicity, likely associated with pore-fluid pressure changes driven by the ascent of magmatic fluids (Ebmeier et al., 2016). The increase in rate and maximum magnitude of the seismic swarms ceased after a M_w 5.6 earthquake which was recorded on 20th October 2014 (Ebmeier et al., 2016). The latter seismic event, however, occurred in a shallow fault and was probably triggered by the deep pressurization related to the ascent of magmatic fluids. This event inhibited the unrest of the volcanic complex and no evidence of surface volcanic activity linked to the seismic swarms has been documented or reported (Ruiz, 2015; Ebmeier et al., 2016).

More recently, another seismic swarm (up to 147,000 events, mainly with M_L < 3.6; IG-EPN, 2019b) occurred from September 2018 to July 2019. Beneath the Chiles-Cerro Negro volcanoes a thick crust is present (up to 60 km; Koch et al., 2021), probably hosting a partially melted volume associated with seismic velocity V_s < 3.2 km/s between 7 and 22 km (Ebmeier et al., 2016; Koch et al., 2021) that could represent crystal-rich magmatic reservoirs ("mush" zones) where the melt fraction might reach up to 14 vol% (Koch et al., 2021).

The tectonic framework of the investigated area is characterised by active NNE trending regional strike-slip faults (Cepeda et al., 1987) with local longitudinal NE- and transversal NW-trending fault systems that cut the volcanoes (Bocanegra and Sánchez, 2017; ICEL, 1983). Of particular interest in terms of the rising of magmas and fluid circulation are the NE-trending Cerro Negro-Nasate and Chiles-Cumbal faults, which run from the Chiles up to the Cumbal volcano (located ca. 15 km to the North; Fig. 1b), and the WNW-trending Chiles-Cerro Negro fault (Bocanegra and Sánchez, 2017) that passes through the homonyms craters and along which the Aguas Hediondas and Aguas Negras

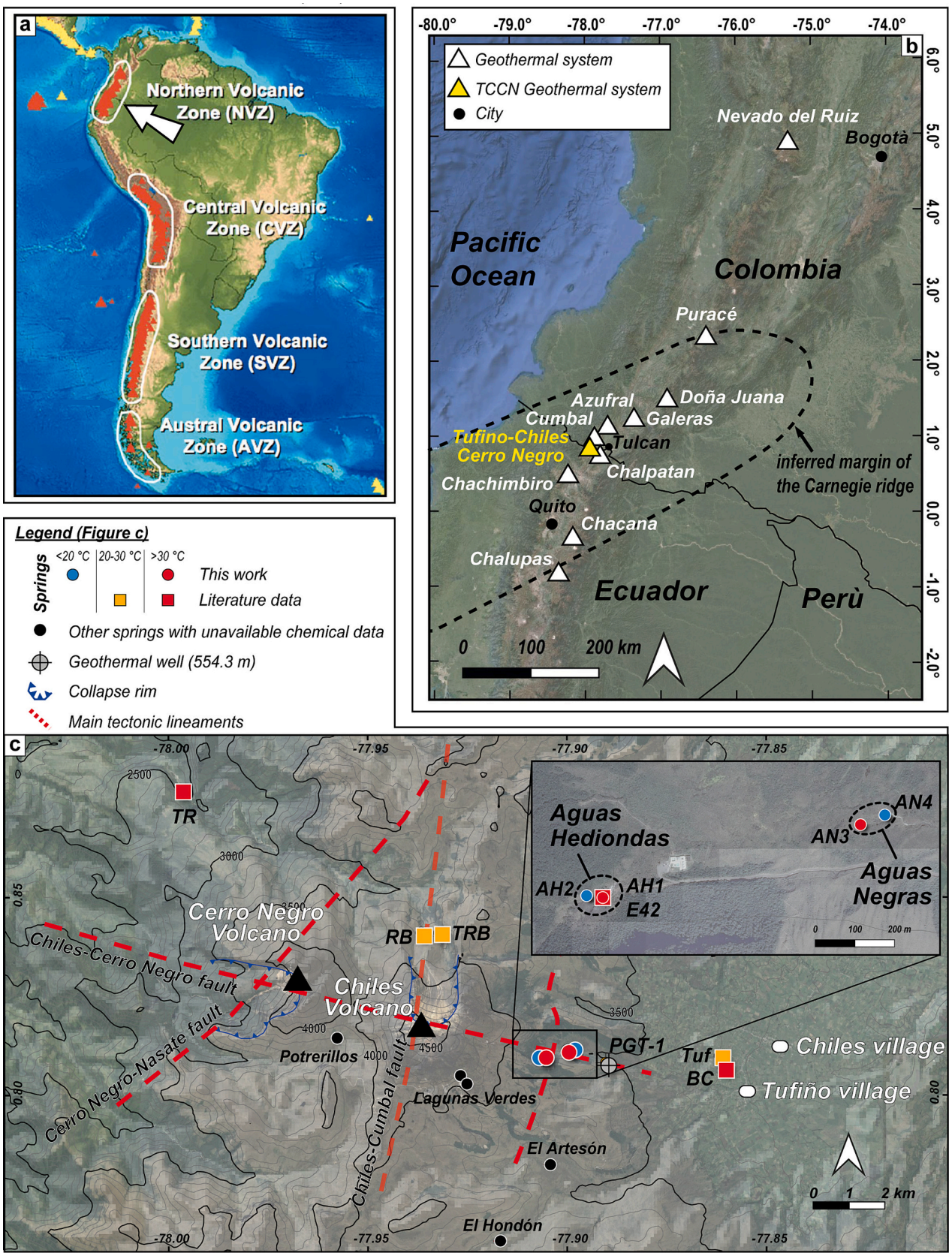

Fig. 1. a) Andean Northern Volcanic Zone in the framework of the Andes Cordillera (modified from Stern, 2004); b) satellite map of the TCCN and the main Ecuadorian and Colombian geothermal systems with depicted the inferred margin of the Carnegie ridge (after Gutscher et al., 1999); c) location of the main thermal springs and pools sampled in this work and from the literature (Carrera and Guevare, 2016; Inguaggiato et al., 2010; SGC, 2020), geothermal well PGT-1 (Espinoza, 2017), other cold and thermal springs in the area (location from IG-EPN, 2014, 2019a) for which chemical data are not available in the literature, and main tectonic lineaments (Ebmeier et al., 2016; Garcia and Sanchez, 2019). Reference system: WGS84.

hydrothermal manifestations are located (Fig. 1c).

2.2. Geothermal background

Water discharges consisting of both acidic hot (up to 55 °C) and near-neutral thermal-hypothermal springs occur 2–3 km East of Chiles volcano and close to the villages of Tufiño and Chiles, respectively (Fig. 1c; Beate and Urquizo, 2015). Strong bubbling gases occur in various hot springs such as Aguas Hediondas and Aguas Negras. Gas geothermometric evaluations from a previous work indicated reservoir temperatures as high as 230 °C (Almeida et al., 1992). Other hot- and cold-water discharges located near both volcanoes are also present (Fig. 1c; Almeida et al., 1992; Cortés and Calvache, 1996; SGC, 2020), and some of them are regularly monitored by the "Instituto Geofísico de la Escuela Politécnica Nacional (IGEPN)" for volcanic surveillance purposes since 2014. Among the latter, IG-EPN reported in 2014 (IG-EPN, 2014) (i.e., the period closest to that of the sampling of the present work) values of temperatures of ~11.0, 42.7, and 39.5 °C, a pH of ~5.7, 5.9 and 6.4, and an electrical conductivity (EC) of ~45, 1518 and 3862 μs/cm for Lagunas Verdes, El Artesón and Potrerillos springs, respectively (Fig. 1c). Recently, a previously unknown thermal water discharge (El Hondón; Fig. 1c) has been discovered at about 6 km SSE of Chiles volcano, where near-neutral pH (values of 7.1 and 7.7), EC of 5766 and 6340 μs/cm and temperature of 85.1 and 85.8 °C were detected in October and December 2019, respectively (IG-EPN, 2019c). Unfortunately, compositional data on all these springs are not available in the literature.

At about 1 km East of the acid springs of Aguas Hediondas and Aguas Negras, fossil silica sinter terraces are indicative of past high-temperature and neutral chloride spring waters (Beate and Urquizo, 2015). Hydrothermal mineralizations near the Aguas Hediondas and Baños de Chiles springs are characterised by cristobalite, tridymite, sulphur, and calcite, gypsum, epsomite, amorphous silica, respectively (Lesmes et al., 2004).

Extensive areas affected by hydrothermal alteration are located inside the craters and about 2.5 km North and 1.5 km South of Chiles volcano, respectively. These areas do not show ground thermal anomalies and likely represent various phases of alteration, among which the most recent seems to be represented by an advanced argillic steam-heated stage (Celec-Isagen, 2015; Espinoza, 2017) where H_2S-rich gas discharges have been recognized (Beate and Urquizo, 2015). Up to date, only one borehole (PGT-1; 3545 m a.s.l.), located about 1.7 km East of Aguas Hediondas (Fig. 1c), was drilled down to a total depth of 554.3 m. The stratigraphic column of this well includes glacial till, andesite-to-rhyodacite lavas, and a thick sequence of low-permeability volcaniclastics (microbreccias) (Beate and Urquizo, 2015; Espinoza, 2017). Two different hydrothermal alteration mineral assemblages were recognized in the PGT-1 borehole by Espinoza (2017). An argillic alteration occurred between 95 and 120 m and between 219 and 255 m below the ground, characterised by smectite, kaolinite, pyrite, and kaolinite, pyrite, sulphur, with minor smectite, respectively. Different assemblages of minerals referred to a sub-propylitic stage, and composed by i) smectite and pyrite, ii) smectite, chlorite and pyrite, and iii) smectite, zeolites, chlorite with minor calcite, were found at 80–95 and 121–165, 165–219, and 255–370 m below the ground, respectively.

The geothermal system possibly consists of two reservoir layers, a deeper one (>1500 m of depth) having temperatures >200 °C, and a shallower one (500–1000 m of depth) with the lower temperature at depth (100–150 °C) (Bona and Coviello, 2016 and references therein; Coviello, 2000; Garcia and Sanchez, 2019). The top of the reservoir is thought to be under Chiles volcano, as inferred from geophysical surveys (Schlumberger and magneto-telluric soundings) (Beate and Urquizo, 2015; INECEL-OLADE-AQUATER, 1987) also indicating the presence of a shallow thick conductive layer (about 100 m) below the acid springs (i.e., Aguas Hediondas and Aguas Negras) which deepens at 400 to 500 m towards the East, where the fault-controlled lateral outflow area is located (i.e., Tufiño village) (Beate and Urquizo, 2015). Based on surface data using the volumetric heat-in-place method, an energy potential of 130–138 MWe was estimated for the Tufiño prospect (Almeida, 1990).

3. Sampling and analytical methods

Four water (AH1, AH2, AN3, AN4) and two gas (AH1 and AN3) samples were collected from the TCCN area (Fig. 1c) in January 2015. These new data were integrated with data already published by Inguaggiato et al. (2010) (1 water sample and 1 bubbling gas sample), Carrera and Guevare (2016) (1 water sample from Baños Tufiño), and the National Inventory of Hydrothermal Manifestations summarised by the Colombia Geological Survey, (SGC, 2020; 4 water samples). Additional data are also reported by Almeida et al. (1992) (23 water and 1 snow samples), although no geographical coordinates are available. Therefore, these latter are used only for a general characterization of the isotopic composition of the waters emerging in the TCCN area and the surroundings. To verify the reliability of the chemical analyses found in the literature, we tested the ionic balance to identify analytical errors at the time of sample selection. The charge balance error accepted was ±10 %. Sampling was carried out following the procedure described by Capaccioni et al. (2014).

Water temperature and pH were measured using a portable instrument (Thermo Scientific™ Eutech™ pH 6+ pH Meter) in the field. Total alkalinity was measured on-site by titration using HCl 0.01 N as titrating agent and methyl-orange as the colorimetric indicator; the error was <5 %. Two water aliquots were collected and filtered at 0.45 μm in the field for the determination of anions and cations. The cation bottle was acidified with Suprapur hydrochloric acid (1 % HCl) to reach a pH value of ~2. An unfiltered water aliquot of 125 mL was sampled for oxygen and hydrogen isotope analysis. An additional unfiltered 500 mL water aliquot was sampled for the analysis of the $^{34}S/^{32}S$ ratio of SO_4^{2-} (expressed as $\delta^{34}S\text{-}SO_4^{2-}$ in ‰ vs. V-CDT). The $\delta^{34}S\text{-}SO_4^{2-}$ values were analysed by mass spectrometry with an EA-IRMS system consisting of a 20–20 isotope ratio mass spectrometer (Europa Scientific, Crewe, UK), equipped with an elemental analyzer (Sercon Ltd., Crewe, UK). The analytical uncertainty was ±0.3 ‰. Main anions (Cl^-, SO_4^{2-}, NO_3^-, Br^-, and F^-) in water samples were analysed by ion chromatography. Ammonia was analysed by molecular spectrophotometry, main cations (Li^+, Na^+, K^+, Ca^{2+}, and Mg^{2+}) by atomic absorption spectroscopy, while H_3BO_3 and SiO_2 by inductively coupled plasma-optical emission spectroscopy. Analytical errors were < 3 % and < 5 % for the main and minor components, respectively (Capaccioni et al., 2014). The isotopic composition of oxygen and hydrogen water samples (expressed as $\delta^{18}O\text{-}H_2O$ in ‰ vs. V-SMOW and $\delta D\text{-}H_2O$ in ‰ vs. V-SMOW, respectively) were determined by mass spectrometry (Vaselli et al., 2006 and references therein), with analytical errors of ±0.05 and ± 1 ‰, respectively.

Bubbling gas samples in water springs were collected employing a plastic funnel positioned above the bubbles and connected with a glass thorion-tapped flask. Inorganic gases (N_2, Ar + O_2, H_2, He, and CO) and CH_4 stored in the soda flask headspace were analysed by using a Shimadzu 15A gas chromatographic system equipped with a 9 m long molecular sieve column and thermal conductivity detector (TCD). Argon and O_2 were analysed using a Thermo Focus gas chromatograph equipped with a 30 m long capillary molecular sieve column and a TCD. Light hydrocarbons were determined by a Shimadzu 14A gas-chromatograph equipped with a 10 m long stainless-steel column (ϕ = 2 mm) packed with Chromosorb PAW 80/100 mesh (coated with 23 % SP1700) and FID detector. Hydrogen sulphide concentrations were determined by analysing sulphate in the soda solution by ion-chromatography after oxidation with H_2O_2, while acidimetric titration with 0.1 N HCl was used to analyse CO_2 dissolved in the soda solution as CO_3^{2-} (Capaccioni et al., 2014; Montegrossi et al., 2001; Nisi et al., 2013; Tassi et al., 2010). The analytical errors were < 5 % for the main gas components and < 10 % for minor and trace gas compounds (Capaccioni et al., 2014; Tassi et al., 2010). Three different gas aliquots were

collected at each sampling point for the determination of stable isotope contents. For the determination of the $^{13}C/^{12}C$ ratios of CO_2 (expressed as $\delta^{13}C\text{-}CO_2$ in ‰ vs. V-PDB) and $^3He/^4He$ values, a pre-evacuated 150 mL glass flask was used. To measure the $^{13}C/^{12}C$ ratios of CH_4 (expressed as $\delta^{13}C\text{-}CH_4$ in ‰ vs. V-PDB) a pre-evacuated 150 mL glass flask filled with 50 mL of a 4 N NaOH solution was sampled, and eventually, a pre-evacuated 60 mL glass flask filled with 20 mL of a 5 N NaOH and 0.15 M $Cd(OH)_2$ suspension was collected for the determination of the chemical composition and the $^{34}S/^{32}S$ ratios in H_2S (expressed as $\delta^{34}S\text{-}H_2S$ in ‰ vs. V-CDT).

A Finnigan Delta S mass spectrometer was used to determine the $\delta^{13}C\text{-}CO_2$ values. The procedure involved a two-step extraction and purification procedure of the gas mixtures by using liquid N_2 and a solid-liquid mixture of liquid N_2 and trichloroethylene. Standards, both Internal (Carrara and San Vincenzo marbles) and international (NBS18 and NBS19), were used to estimate external precision. The analytical uncertainty and the reproducibility were ± 0.05 ‰ and ± 0.1 ‰, respectively (Capaccioni et al., 2014). The $\delta^{13}C\text{-}CH_4$ value at Aguas Negras was determined by mass spectrometry using a Varian MAT 250, according to the procedure reported by Schoell (1980). The analytical uncertainty was ±0.15 ‰. The sulphur isotopic content of H_2S was determined with the same instrument used for the analysis of the $\delta^{34}S\text{-}SO_4^{2-}$ values after oxidising the CdS precipitate with H_2O_2. The $^3He/^4He$ ratios were determined by using a double collector mass spectrometer (VG 5400-TFT) following the procedure defined by Inguaggiato and Rizzo (2004), with an analytical uncertainty of ±1 %. The helium isotopic compositions are expressed as R/Ra, with R representing the $^3He/^4He$ measured ratio in the sample and Ra as the $^3He/^4He$ ratio in the air (1.39×10^{-6}; Mamyrin and Tolstikhin, 1984).

4. Results

4.1. Chemical and stable isotope composition of waters

The temperature, pH value, and chemical and isotopic composition of water samples analysed in this work and from previously published studies are shown in Table 1. The water temperatures range from 8.6 to 54.7 °C, thus can be classified as cold (<20 °C), hypothermal (20–30 °C), and thermal (>30 °C) waters, considering that the mean annual temperature in the Carchi Province (Ecuador) is ~15.5 °C (climateknowledgeportal.worldbank.org). Most waters had temperatures >20 °C, with the hottest (AH1, E42: 52.5–54.7 °C) and the colder (AH2: 8.6 °C) ones measured at Aguas Hediondas from springs occurring just tens of metres far away from each other (Fig. 1c). All water samples from the TCCN area show slightly acid to neutral pH, ranging between 4.52 and 6.58, with the most acid value measured at Aguas Hediondas (AH1). Total Dissolved Solids (TDS), determined as the sum of the major components and silica, span over a wide range of values from 33.6 mg/L measured in the coldest spring (AH2), up to 3095 mg/L of the Termal del Rio (TR; Fig. 1c) spring, which is the farthest one from the Chiles volcano (9.5 km NW).

Among the major cations, Na^+ and Mg^{2+} usually range between 2.2 mg/L (AH2) and 430 (TR) mg/L and 1.8 mg/L (AH2) and 99 mg/L (TR), respectively. Calcium is always present in subordinate amounts, but occasionally dominates (RB, TRB), and generally ranges from 2.8 mg/L (AH2) up to 412 mg/L (TRB), while K^+ ranges between 1.0 mg/L (AH2) and 45 mg/L (AH1). Concerning the main anions, SO_4^{2-} is present in all the waters and usually dominates in thermal and hypothermal springs (AH1, E42, AN3, RB, TRB), ranging from 10 mg/L (AH2) and 1040 mg/L (RB). Bicarbonate is the dominant anion in the coldest spring (AH2: 16 mg/L) and in the farthest samples (TR, Tuf, BC) where it reaches 1650 mg/L (TR) but was not detected in the AN4 and E42 samples (d.l. < 10 mg/L). Cl^- ranges from 0.1 mg/L (AH2) up to 287 mg/L (TR), showing similar values in both Aguas Hediondas and Aguas Negras thermal springs (i.e., 110 and 116 mg/L, respectively).

Fluoride, Br^- and NO_3^- analysis, when analyses are available, range between 0.03 mg/L (AH2) and 4.4 mg/L (E42), 0.23 mg/L (AN3) and 2.4 mg/L (E42), and 0.02 mg/L (AN4) and 8.8 mg/L (TR), respectively. Lithium, NH_4^+, and B range between 0.10 mg/L (AN3) and 1.50 mg/L (TRB), 0.02 mg/L (AN4) and 1.40 mg/L (AH1), and 0.3 mg/L (RB) and 21 mg/L (TR), respectively. Silica content varies from 62 mg/L and 165 mg/L, the highest value being recorded in the Baños Chiles area (BC), whereas the lower one corresponds to the sample RB located in the Rio Blanco area.

The $\delta D\text{-}H_2O$ and $\delta^{18}O\text{-}H_2O$ values for thermal and cold waters range from −104.1 ‰ (Sample ECU216; Almeida et al., 1992) to −66.8 ‰ (TR) and − 14.9 ‰ (Sample ECU216; Almeida et al., 1992) to −8.30 ‰ (TR) vs. V-SMOW, respectively. The snow sample collected in Chiles Volcano (Almeida et al., 1992) shows values for $\delta D\text{-}H_2O$ and $\delta^{18}O\text{-}H_2O$ of −181.7 ‰ and − 23.6 ‰ vs. V-SMOW, respectively. Sample data are reported in the $\delta D\text{-}H_2O$ versus $\delta^{18}O\text{-}H_2O$ diagram, along with the Local Meteoric Water Line (LMWL; data from IAEA network Ecuadorian stations of Lago Agrio, Izobamba, Quito-INHAMI; https://nucleus.iaea.org/wiser) and Global Meteoric Water Line (GMWL; Craig, 1961) (Fig. 2). Samples from this study (circles) and previous works (squares and triangles) fit on the LMWL, except for a moderate shift for a cold water sample from Almeida et al. (1992) and the TR sample which presents a greater deviation from the LMWL.

Sulphur stable isotopes ($\delta^{34}S\text{-}SO_4$) were analysed only in two samples of the present study. Values are +19.23 and + 19.24 ‰ vs. V-CDT, from samples AH1 and AN3, respectively.

4.2. Chemical and stable isotopic composition of bubbling gases

The chemical compositions of inorganic and organic (C2-C6 hydrocarbons) fractions in the bubbling gases from samples AH1 and AN3, along with their isotopic contents, are reported in Table 2. The gas discharges of the investigated areas consisted of bubbling pools, hence it is not surprising that acidic and high-soluble gases (i.e. SO_2, HF, HCl) were not detected. The gas chemical composition of the two samples is similar and is dominated by CO_2 (961 to 964 mmol/mol) followed by N_2 (21 to 26 mmol/mol), H_2S (11 to 13 mmol/mol), O_2 (0.66 to 0.72 mmol/mol) and Ar (0.48 to 0.62 mmol/mol), with minor amounts of H_2 (0.061 to 0.075 mmol/mol), CH_4 (0.036 to 0.041 mmol/mol) and CO (0.031 to 0.036 mmol/mol). Ne and He show similar concentrations as well, ranging from 0.26 to 0.31 μmol/mol and 0.13 to 0.15 μmol/mol, respectively. Organic compounds such as ethane (C_2H_6), propane (C_3H_8), and benzene (C_6H_6) show concentrations ranging from 0.15 to 0.21 μmol/mol, 0.06 to 0.07 μmol/mol, and 0.09 to 0.11 μmol/mol, respectively.

The $\delta^{13}C\text{-}CO_2$ values range from −5.3 ‰ to −6.2 ‰ vs.V-PDB while helium ratios, corrected for air contamination (Rc/Ra), indicate a significant contribution from the mantle at Aguas Negras (5.88 Ra) and, to a lesser extent, at Aguas Hediondas (3.13 Ra). The only $\delta^{13}C\text{-}CH_4$ value was measured in sample AN3, showing a value of −44.5 ‰ vs. V-PDB. The $\delta^{34}S\text{-}H_2S$ values in both the gas samples are +6.67 ‰ to +10.67 ‰ vs. V-CDT, for AN3 and AH1, respectively.

5. Discussion

5.1. Processes controlling the chemical and isotopic composition of waters

According to the $\delta^{18}O\text{–}H_2O$ and $\delta D\text{-}H_2O$ binary diagram (Fig. 2a, b), where the LMWL ($\delta D = 8.18\delta^{18}O + 12.67$; https://nucleus.iaea.org/wiser) and the GMWL ($\delta D = 8.0\delta^{18}O + 10$; Craig, 1961) are reported, the TCCN waters have a meteoric origin, similarly to the Cumbal and Galeras springs (Fischer et al., 1997; Lewicki et al., 2000). Only samples from Aguas Hediondas (AH1-E42) and the north-western part of the geothermal system (TR) plots slightly off the LMWL (Fig. 2b). The slight ^{18}O enrichment observed in the Aguas Hediondas thermal waters was likely due to water-rock interactions. In the same way, sample TR, showing enrichment of $\delta^{18}O\text{–}H_2O$ from the LMWL roughly follows the

Table 1
Chemical and stable isotopic composition of cold and thermal waters from the TCCN area. Geographic coordinates (Ref. Sys.: WGS84), date of sampling, elevation, pH values and outlet temperature are also reported.

ID	Type	Site	Lat.	Lon.	Altitude	Date	T	pH	TDS	Cl^-	SO_4^{2-}	HCO_3^-	F^-	Br^-	NO_3^-	Ca^{2+}	Mg^{2+}	Na^+	K^+	SiO_2	Li^+	NH_4^+	B	C.B.E.	$\delta D\text{-}H_2O$	$\delta^{18}O\text{-}H_2O$	$\delta^{34}S\text{-}SO_4$
					m a.s.l.	dd.mm.yy.	°C		mg/L	mg/L	mg/L	mg/L	mg/L	mg/L	mg/L	mg/L	mg/L	mg/L	mg/L	mg/L	mg/L	mg/L	mg/L	%	‰ vs. V-SMOW		‰ vs. V-CDT
AH1[a]	TS	Aguas Hediondas	0.80974	−77.90597	3608	15.01.2015	54.7	4.52	1273	109.5	668.4	13.7	2.98	0.29	bdl	86.4	53.0	195.9	45.1	98.2	0.26	1.40	5.6[e]	+ 3.1	−88.08	−11.76	+19.23
AH2[a]	CS	Aguas Hediondas	0.80976	−77.90632	3613	15.01.2015	8.6	5.39	34	0.1	10.0	15.7	0.03	bdl	bdl	2.8	1.8	2.2	1.0	na	bdl	bdl	na	−6.7	−81.30	−11.52	na
AN3[a]	TS	Aguas Negras	0.81139	−77.90013	3544	16.01.2015	35.7	5.77	1479	116.3	538.5	326.9	0.41	0.23	bdl	104.9	78.1	142.0	33.5	138.4	0.10	0.65	4[e]	−3.0	na	na	+19.24
AN4[a]	CP	Aguas Negras	0.81160	−77.89957	3544	16.01.2015	19.0	5.15	1234	110.5	771.8	bdl	0.66	0.27	0.02	102.3	76.9	137.0	34.1	na	0.13	0.02	na	−2.5	na	na	na
E42[b]	TS	Aguas Hediondas	0.80966	−77.90592	3601	26.02.2009	52.5	4.60	1327	123.7	816.1	nr	4.37	2.40	nr	91.0	48.0	201.2	40.3	nr	0.28	nr	nr	−5.7	−87.00	−11.7	nr
Tuf[c]	IS	Tufiño	0.80989	−77.86176	3279	25.10.2014	25.0	6.58	687	90.9	140.8	270.5	nr	nr	1.00	45.3	44.5	69.6	24.4	nr	nr	nr	0.2	−1.8	nr	nr	nr
RB[d]	IS	Rio Blanco	0.84111	−77.93662	3749	09.09.2012	20.4	5.31	1780	3.4	1042.8	229.6	nr	nr	nr	362.0	43.6	30.8	5.9	61.5	nr	nr	0.3	−5.0	−89.76	−12.55	nr
TRB[d]	IS	Termal Rio Blanco	0.84106	−77.93215	3771	09.09.2012	24.5	5.44	1802	7.3	964.0	254.0	nr	nr	8.78	412.0	50.7	32.8	7.7	64.5	nr	nr	2.4	+3.8	−89.80	−12.63	nr
BC[d]	IS	Baños Chiles	0.80706	−77.86067	3271	26.10.2011	36.0	6.26	1414	70.5	195.7	695.4	0.39	nr	nr	85.0	63.5	115.5	23.0	165.2	nr	nr	2.2	−7.3	−89.57	−12.42	nr
TR[d]	TS	Termal del Rio	0.87715	−77.99701	2430	10.09.2012	32.9	6.58	3095	287.3	310.3	1652.0	nr	nr	0.8	182.0	99.2	430.0	31.8	102.0	1.50	nr	21.1	−6.2	−66.75	−8.40	nr

TS: thermal spring; CS: cold spring; CP: cold pool; IS: hypothermal spring;
C.B.E.: Charge Balance Error = $\sum$cations−$\sum$anions / $\sum$cations+$\sum$anions × 100
nr: not reported; bdl: below detection limit; na: not analysed.
SGC (2020) identification codes: RB = 41,552 I; TRB = 41,551 I; BC = 36,266 I; TR = 41,553 I
[a] This work.
[b] Inguaggiato et al. (2010).
[c] Carrera and Guevara, 2016).
[d] SGC (2020).
[e] B concentration converted from H_3BO_3.

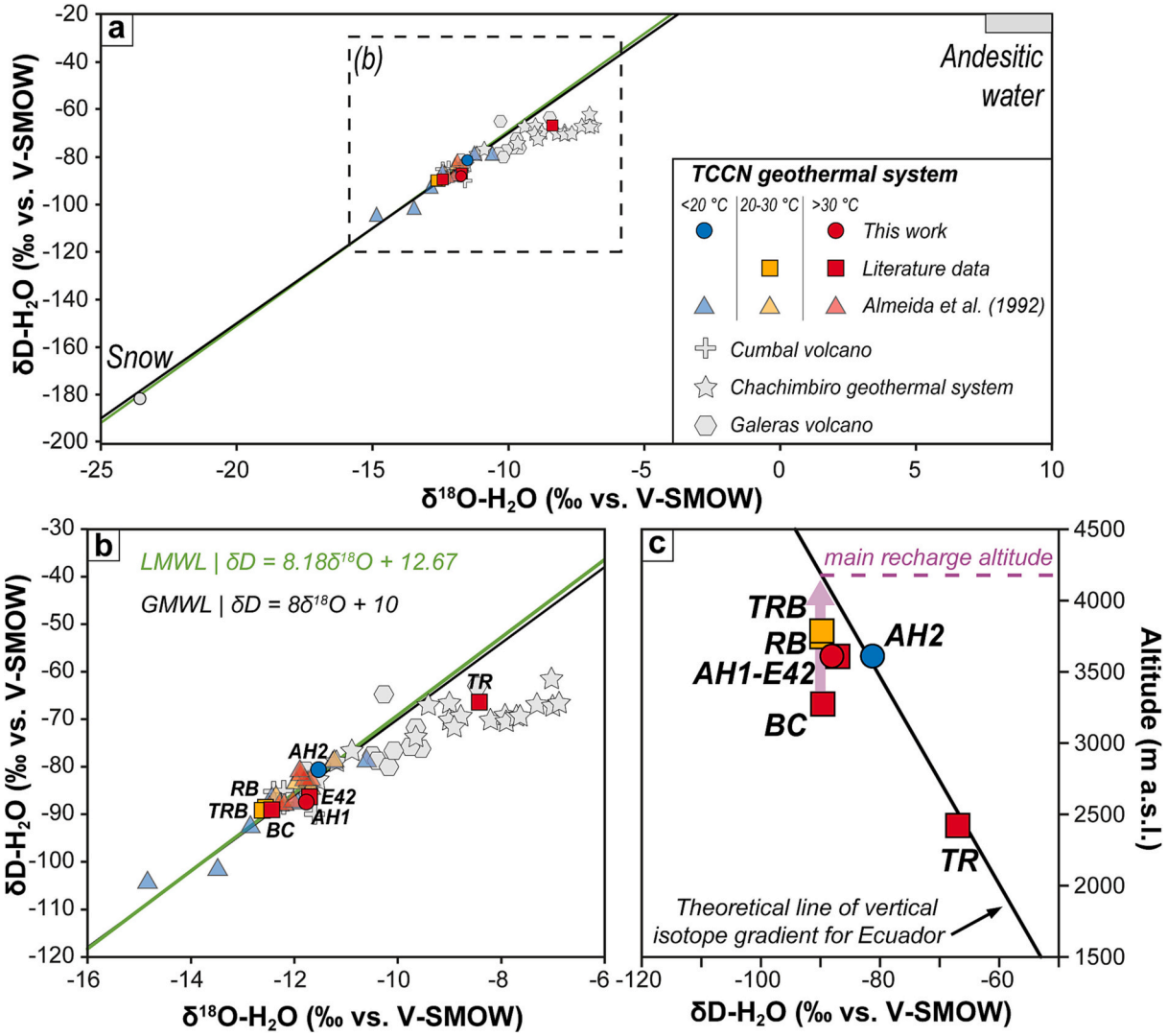

Fig. 2. a) and b) δD-H_2O versus $\delta^{18}O$-H_2O for the TCCN water samples. The Global Meteoric (GMWL; Craig, 1961) and Local Meteoric Water Lines (LMWL; data from IAEA network; https://nucleus.iaea.org/wiser) have been reported. c) Elevation of TCCN waters versus δD isotopic composition. The theoretical line of vertical isotope gradient for Ecuador is from Inguaggiato et al. (2010). Data from Cumbal (Lewicki et al., 2000) and Galeras (Fischer et al., 1997) volcanoes, and Chachimbiro geothermal system (Aguilera et al., 2005) are also plotted for comparison.

trend defined by the Chachimbiro waters (Aguilera et al., 2005). When the δD-H_2O values are combined with the elevation of each water discharge, the TR and AH2 waters plot along the theoretical line of vertical isotope gradient for Ecuador (Inguaggiato et al., 2010) suggesting a common recharge area. Differently, the other thermal and hypothermal waters of the TCCN (AH1, E42, TRB, RB, and BC) plot in correspondence to an altitude of about 4100–4200 m a.s.l., i.e. ~500 m (TRB, RB) up to ~1000 m (BC) higher than their elevation, indicating that Chiles volcano (~4700 m a.s.l.) is the main recharge area feeding these springs.

Waters from TCCN with temperature up to 54.7 °C, present a slightly acid to neutral pH value and variable TDS concentrations (687 to 3095 mg/L) that generally increase at increasing temperatures (Fig. 3). Samples from Aguas Hediondas (AH1, E42), however, deviate from this general positive correlation, showing the highest outlet temperatures at intermediate TDS contents (1172–1320 mg/L).

In the HCO_3-Cl-SO_4 ternary diagram (Fig. 4) all the samples fall far from the "mature waters" field, being characterised by SO_4- or HCO_3-dominated composition. In general, waters from the TCCN roughly resemble those from the Cumbal and Galeras active volcanoes (Fischer et al., 1997; Lewicki et al., 2000), while are markedly different from those of the Chachimbiro geothermal system (Aguilera et al., 2005). The acid sulphate composition shown by the thermal waters from Aguas Hediondas (AH1, E42) and Aguas Negras (AN3) and hypothermal waters located on the northern side of Chiles volcano (TRB, RB) is typically produced by absorption of sulphur-bearing gases (H_2S) into the shallow aquifers (Ellis and Mahon, 1977; Giggenbach, 1988; Lewicki et al., 2000), likely related to the highest portions of the geothermal reservoir. The chemistry of these waters is in agreement with the advanced argillic steam-heated alteration stage recognized in this area (Celec-Isagen, 2015; Espinoza, 2017). Considering their intermediate TDS (Fig. 3), these thermal and hypothermal waters seem to be associated with a relatively shallow and short hydrogeological circulation, as also supported by the low tritium values recorded by Almeida et al. (1992). Moreover, the negative correlation between SO_4^{2-} and SiO_2 shown by the TCCN samples (Fig. 5), coupled with a general increase in pH, supports the theory of a progressive isochemical dissolution of the host rocks due to the acidic and immature nature of these waters.

The coldest water (AH2) and the thermal/hypothermal waters of Baños de Chiles (BC), Tufiño (Tuf), and Termal del Rio (TR) display a predominance of HCO_3^- with subordinate Cl^- and SO_4^{2-}. The HCO_3^- in geothermal waters is commonly produced by the reaction of CO_2-rich

Table 2
Chemical and stable isotopic composition of bubbling gas samples.

ID	Type	Site	H_2	O_2	N_2	CO	CH_4	CO_2	He	Ne	H_2S	Ar	C_2H_6	C_3H_8	C_6H_6	$\delta^{13}C$-CO_2	$\delta^{13}C$-CH_4	$\delta^{34}S$-H_2S	R/Ra	Rc/Ra	$CO_2/^3He$
			mmol/mol	mmol/mol	mmol/mol	mmol/mol	mmol/mol	mmol/mol	mmol/mol	mmol/mol	mmol/mol	mmol/mol	mmol/mol	mmol/mol	mmol/mol	‰ vs. V-PDB		‰ vs. V-CDT			
AH1	BG	Aguas Hediondas	0.075	0.72	21	0.031	0.036	964	0.00013	0.00026	13	0.48	0.00021	0.00006	0.00011	−5.28	nd	+10.67	2.4	3.13	2.21E+12
AN3	BG	Aguas Negras	0.061	0.66	26	0.036	0.041	961	0.00015	0.00031	11	0.62	0.00015	0.00007	0.00009	−6.22	−44.5	+6.67	4.6	5.88	9.95E+11

BG: bubbling gas
na: not analysed
N_2/Ar: AH1 = 43.7; AN3 = 41.9

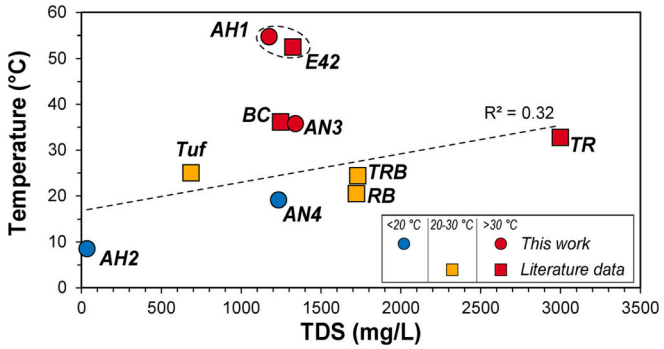

Fig. 3. Total Dissolved Solid (TDS) content (mg/L) vs. water temperatures (°C) in the TCCN samples.

fluids with Na—K silicates, by the dissolution of carbonates, or by the direct dissolution of CO_2 in water. In TCCN, besides sample AH2 which, considering its low TDS and the chemical and isotopic characteristics can be regarded as a surface meteoric-in-origin water, HCO_3-dominate waters show medium-to-high TDS values (Tuf = 687 mg/L; BC = 1250 mg/L; TR = 3095 mg/L) and have a Na-HCO_3 or (subordinately) Mg-HCO_3 hydrofacies (Fig. 4). Moreover, an excess of HCO_3^- with respect to Ca^{2+} ($HCO_3^-/Ca^{2+} > 1.96$ normal ratio), Na^+ ($HCO_3^-/Na^+ > 1.45$ normal ratio) and Mg^{2+} ($HCO_3^-/Mg^{2+} > 1.21$ normal ratio) is found in all these waters. These characteristics were likely produced by the interaction of CO_2-bearing fluids with silicate rocks and, considering their spatial location (Fig. 1c), these waters can be regarded as peripheral waters of the geothermal system.

Concerning minor components, Li^+ vs. B concentrations and Li^+ vs B vs Cl^- are reported in Fig. 6. Lithium is generally released during water-rock interactions and is strictly dependent on the temperature (e.g., Fouillac and Michard, 1981); whereas B may indicate the occurrence of a vapour phase, or from evaporites, although the latter hypothesis is unlikely since no evaporitic deposits were recognized in the stratigraphic sequence of TCCN (Beate and Urquizo, 2015). In Fig. 6, samples AH1, AN3 and TR are shown in a Cl-B-Li triangular plot, suggesting absorption of a steam phase presenting a normalised B slightly dominant compared to normalised Cl^- (Giggenbach, 1991). Sample TR, located to the northwest of Cerro Negro, shows the highest B/Cl steam absorption.

The measured sulphur isotopes ($\delta^{34}S$-SO_4) values for AH1 and AN3 water samples show positive values of +19.23 and + 19.24 ‰ vs. V-CDT higher than those recorded in H_2S in gas samples (Table 2). These highly positive values strongly differ from those typical of volcanic origin (i.e., +0.7 to +1.0 ‰ vs. V-CDT; Marini et al., 2011), while being similar to that measured at Chachimbiro (i.e., +13.66 ‰ vs. V-CDT; Aguilera et al., 2005). These high values can be related to evaporite deposits (e.g., Capaccioni et al., 2014), though previously published geological and stratigraphical works in the area do not report the presence of evaporites in the volcanic basement (Beate and Urquizo, 2015). However, the highly positive $\delta^{34}S$-SO_4 values of the TCCN also approach those related sulphate entrapped during subduction (i.e., +17.5 ± 3.5 ‰ vs. V-CDT; Kagoshima et al., 2015) and then recycled during physico-chemical processes in which the subducted slab is generally involved.

5.2. Origin of gases

Helium, N_2, and Ar are plotted in a ternary diagram (Fig. 7) and used as a source indicator for the origin of volatile components (after Giggenbach and Goguel, 1989). The N_2/Ar ratios of the bubbling gas samples AH1 and AN3 vary between a very tight range (42 to 44; Table 2). Both samples fit close to the Air-Saturated Water ("ASW") value of 38, therefore indicating that both N_2 and Ar have a dominant atmospheric origin, which is consistent with an important contribution of the meteoric component to water composition, as shown by stable isotopes in

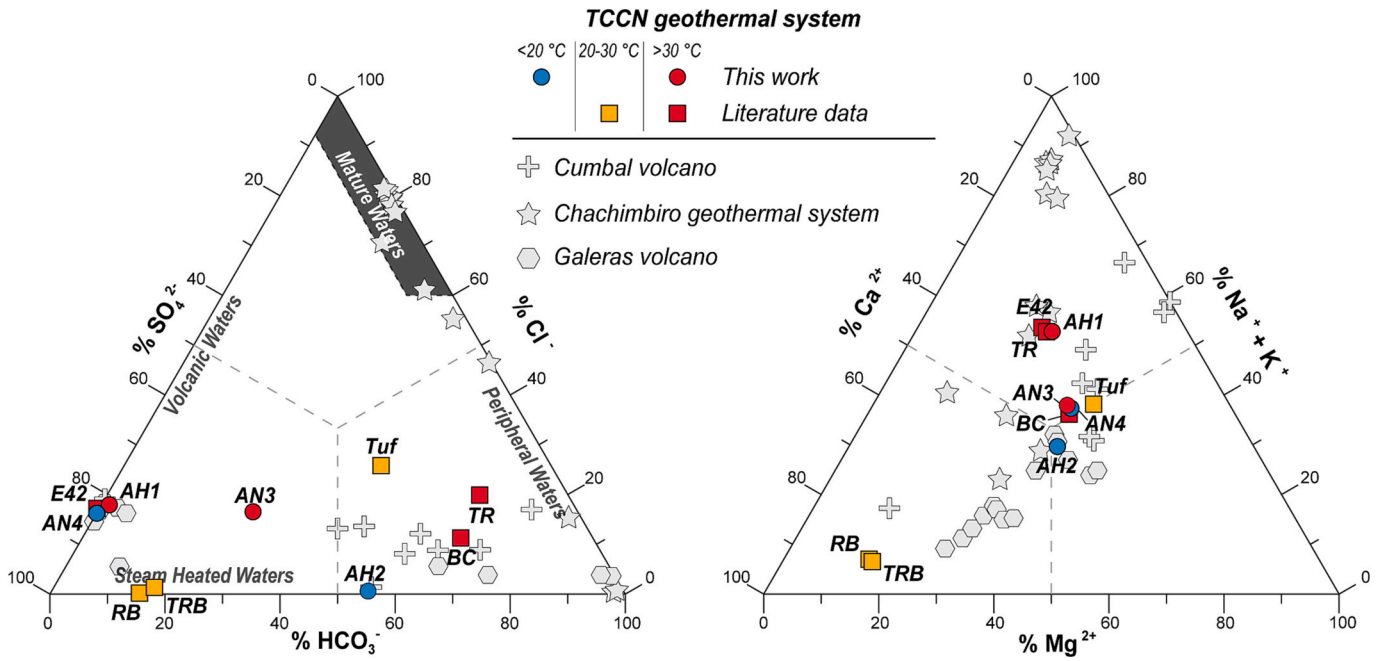

Fig. 4. $HCO_3^- - Cl^-$- SO_4^{2-} and Ca^{2+}- $(Na^+ + K^+)$ - Mg^{2+} ternary diagrams for cold (<20 °C), hypothermal (20–30 °C) and thermal (>30 °C) waters from the TCCN area. Data from the Chachimbiro geothermal system (Aguilera et al., 2005) Cumbal (Lewicki et al., 2000) and Galeras volcanoes (Fischer et al., 1997) are also reported for comparison. Data in meq/L are plotted as relative proportion in %.

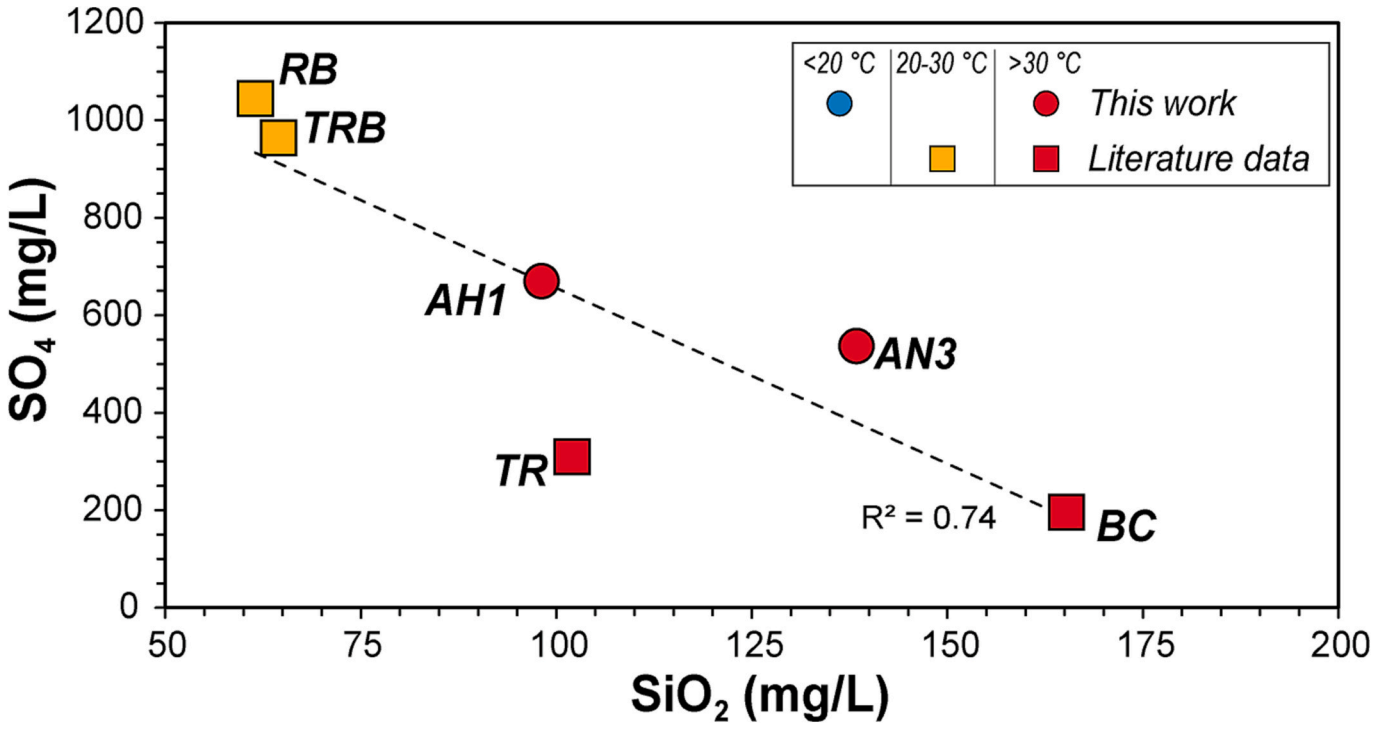

Fig. 5. SO_4^{2-} vs. SiO_2 content (both in mg/L) in the TCCN samples.

Fig. 2.

As shown in Fig. 8, the $^3He/^4He$ ratios (R/Ra) of samples AH1 and AN3 range between 2.4 and 4.6 (i.e., 3.13 and 5.88 Rc/Ra), respectively (Table 2), indicating a notable mantle He contribution (R/Ra = Rc/Ra = 7.2 and 8.5 Ra for Ecuadorian and Colombian mantle, respectively; Lages et al., 2021; Fig. 8), diluted by the addition of radiogenic and/or atmospheric ^4He. The mixing hyperbolas plotted in Fig. 8 suggest that the He isotopic composition of AN3 and AH1 bubbling gases results from mixing between deep-seated fluids containing He with R/Ra values between 3Ra and 6Ra, either air (R/Ra = 1.0 and $^4He/^{20}Ne = 0.3185$) or meteoric water containing dissolved atmospheric He at ASW conditions and a crustal component (R/Ra = ~0.05; Shaw et al., 2003). The lower values compared to the Colombian and Ecuadorian mantle R/Ra estimated ratios presented by Lages et al. (2021), are indicative of variations in the degree of crustal contamination for radiogenic ^4He addition.

Crustal contamination of mantle-derived fluids can modify the

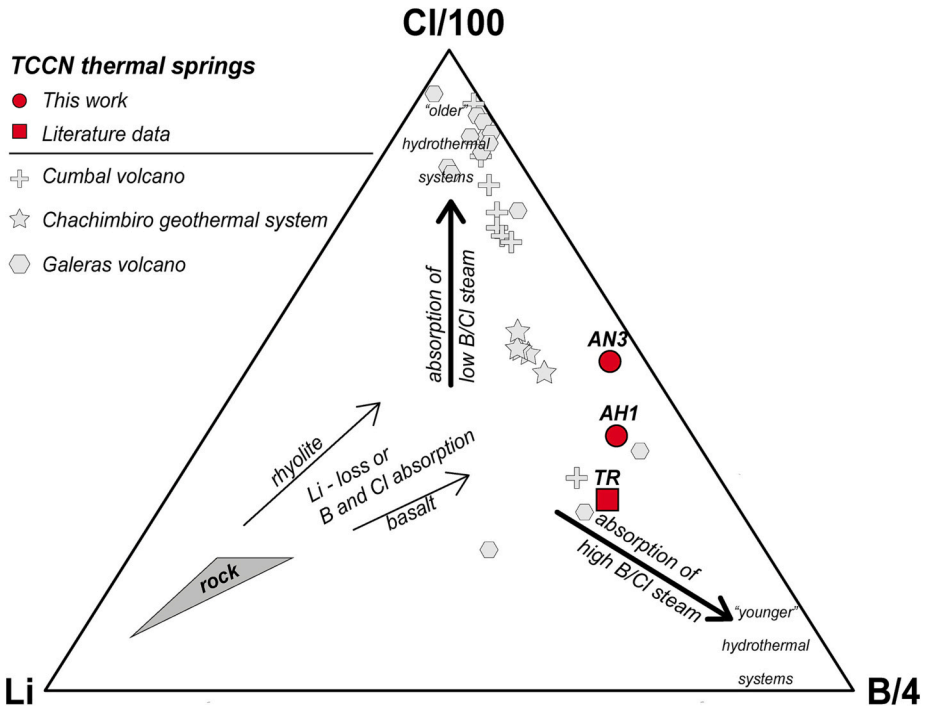

Fig. 6. $Cl^{-}/100$, Li^{+}, B/4 ternary diagram (Giggenbach, 1991) for the thermal waters from the TCCN. Data from the Chachimbiro geothermal system (Aguilera et al., 2005) Cumbal (Lewicki et al., 2000) and Galeras volcanoes (Fischer et al., 1997) are also reported for comparison.

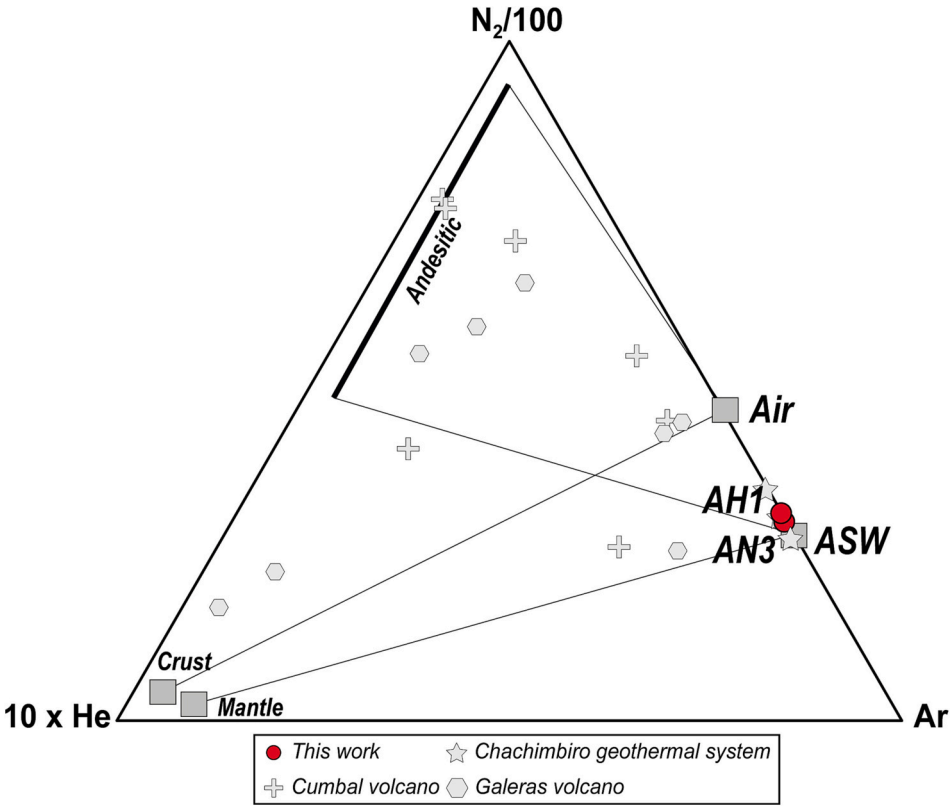

Fig. 7. Ar–N_2–He ternary diagram for gas samples. Air Saturated Water (ASW), Air, Crust, Mantle, and Andesitic values are after Giggenbach et al. (1993). Data from the Chachimbiro geothermal system (Aguilera et al., 2005) Cumbal (Lewicki et al., 2000) and Galeras volcanoes (Fischer et al., 1997) are also reported for comparison.

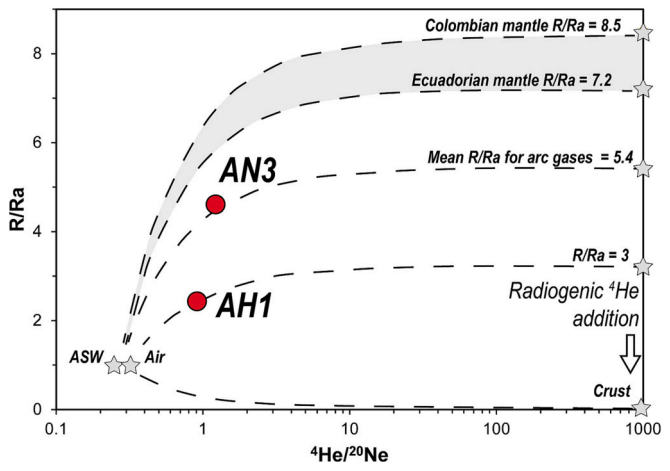

Fig. 8. R/Ra versus $^{4}He/^{20}Ne$ of Aguas Hediondas and Aguas Negras samples. The Ecuadorian and Colombian mantle, crust, Air and Air-Saturated Water (ASW) endmembers are reported. Dashed lines represent mixing curves between Colombian and Ecuadorian mantle (Lages et al., 2021), mean R/Ra for arc gases (Hilton et al., 2002), crust (Shaw et al., 2003), and ASW endmembers (after Tardani et al., 2021).

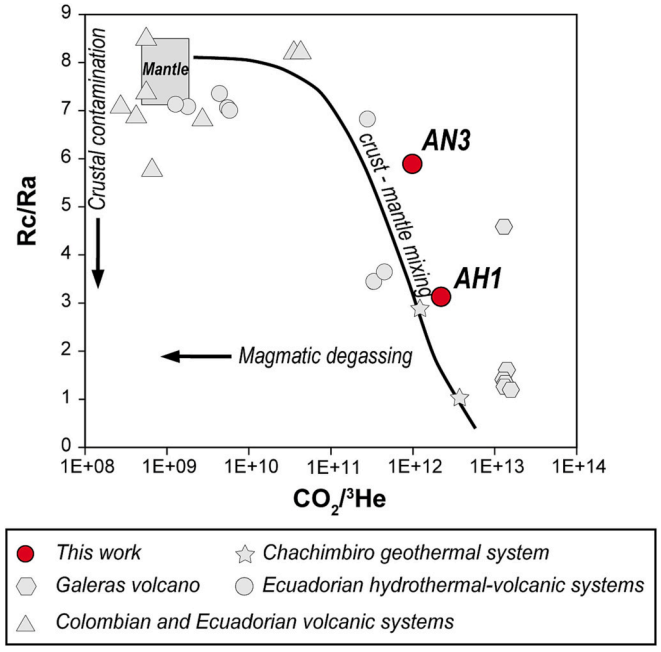

Fig. 9. $CO_2/^{3}He$ vs. Rc/Ra of TCCN samples compared with the fluids of the Andean Northern Volcanic Zone; crust-mantle binary mixing line (in black) assumes an Rc/Ra of 8.5 (after Lages et al., 2021). Data from the Chachimbiro geothermal system (Aguilera et al., 2005), Galeras volcano (Fischer et al., 1997; Sano et al., 1997), Ecuadorian hydrothermal systems (Inguaggiato et al., 2010) and Colombian and Ecuadorian volcanoes (Lages et al., 2021) are also reported for comparison.

$^{3}He/^{4}He$, $CO_2/^{3}He$ ratios, and $\delta^{13}C–CO_2$ values through the addition of radiogenic ^{4}He and CO_2 from crustal rocks (Sano et al., 1998). When the $CO_2/^{3}He$ ratio is plotted against the related Rc/Ra value (Fig. 9), both bubbling gas samples (AH1, AN3) lie on a mixing line between mantle and crust values (Lages et al., 2021) with Rc/Ra lower than the mantle value estimated for Colombia and Ecuador (8.5 and 7.2 Ra, respectively; Lages et al., 2021) and $CO_2/^{3}He$ ratios (AH1: 2.2×10^{12}; AN3: 9.9×10^{11}) higher than mantle value (1.5×10^{9}; Sano and Marty, 1995). The high $CO_2/^{3}He$ ratios and the Rc/Ra values indicate a considerable contribution of crustal-derived fluids, with CO_2 and radiogenic ^{4}He addition in the hydrothermal system. As suggested by Giggenbach et al. (1993), the carbon and radiogenic He excess is most likely derived from marine sediments carried to the zones of arc magma generation on top of the subducted slab. The composition of the subducted component would correspond to that of a gas with a crustal $^{3}He/^{4}He$ ratio and a very high $CO_2/^{3}He$ ratio.

Further suggestions concerning the origin of carbon in hydrothermal fluids are provided by the three-component mixing model proposed by Sano and Marty (1995). Based on their $CO_2/^{3}He$ and $\delta^{13}C–CO_2$ ratios, samples are described by a carbon mixture made of marine carbonates, mantle, and organic sediments. The $\delta^{13}C–CO_2$ of the Colombian and Ecuadorian mantle was not reported by Lages et al. (2021), thus a value of -6.5 ± 2.5 ‰ vs. V-PDB (Sano and Marty, 1995; Sano and Williams, 1996) was considered for the mantle component. In contrast, $\delta^{13}C–CO_2$ of sediments varies between two major components (Hoefs, 2009): organic sediments (−40 ‰ to −20 ‰ vs. V-PDB) and marine limestones (0 ± 2 ‰ vs. V-PDB). According to Fig. 10, the investigated gas samples plot near the limestone endmember, on a theoretical vertical lineament determined by Galeras and Chachimbiro thermal springs and other samples from Ecuadorian hydrothermal systems. It is worth noting that the TCCN system lies on the subducting Carnegie ridge (Fig. 1b) that is covered by a thick sedimentary sequence of upper Miocene-to-upper Pleistocene age (Hidalgo et al., 2012 and references therein). These sediments are mainly composed of nannofossil ooze with diatoms and clays, and in minor proportion by radiolarians, silicoflagellates, and pyrite (Mix et al., 2003). Additionally, the top of the Carnegie ridge contains multi-kilometres-wide, sub-circular depressions carved into the carbonate blanket that covers the ridge (Michaud et al., 2005), which might explain the $CO_2/^{3}He$ and $\delta^{13}C–CO_2$ values approaching the limestone component. The slight shifting of gas compositions related to the mantle-limestone mixing curve may suggest a modest contribution of biogenic carbon or secondary processes such as calcite precipitation, which might occur in the shallow aquifer and produce more negative

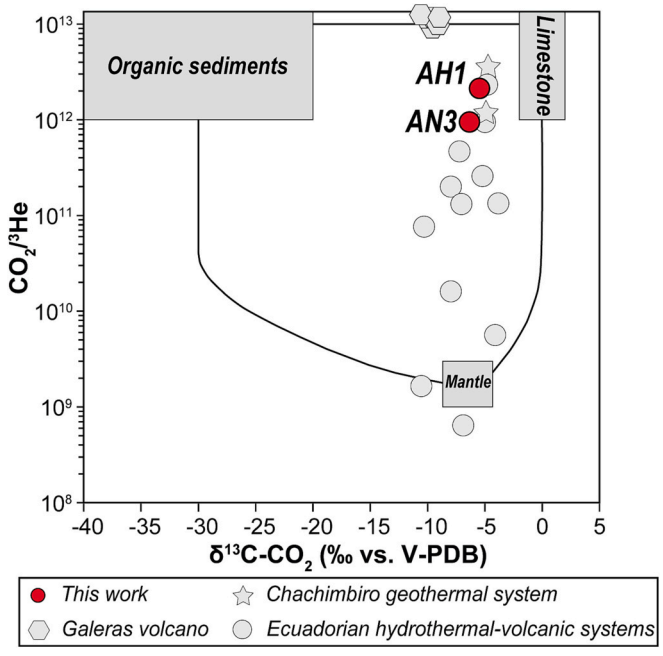

Fig. 10. Correlation diagram of $CO_2/^{3}He$ vs. $\delta^{13}C$-CO_2 (‰ vs. V-PDB) for TCCN gas samples. Model end-members of mantle, marine limestone and organic sediment arc are also indicated. Lines show mixing lines among the end-members (after Sano and Marty, 1995). Data from the Chachimbiro geothermal system (Aguilera et al., 2005), Galeras volcano (Sano et al., 1997) and Ecuadorian hydrothermal systems (Inguaggiato et al., 2010) are also reported for comparison.

values of the $\delta^{13}C–CO_2$ (Barry et al., 2022; Hilton et al., 1998; Tardani et al., 2016).

Regarding CH_4, useful information to investigate the origin of this gas in hydrothermal and volcanic environments (e.g., Giggenbach et al., 1993; Giggenbach, 1995; Poreda et al., 1988; Tassi et al., 2010) can come from the $CH_4/^3He$ ratio. In the AN3 and AH1 gases, these ratios are equal to 4.3×10^7 and $8.3 \times 10,^7$ respectively, and are comprised between abiotic (between 1×10^5 and 1×10^6) and thermogenic (up to 1×10^{12}) values (Poreda et al., 1988; Snyder et al., 2003). Thermogenic, biogenic, and volcanic-hydrothermal CH_4 can also be distinguished through the $CH_4/(C_2H_6 + C_3H_8)$ ratios (Bernard et al., 1978). Although isotopic fractionation processes might occur in changing the $\delta^{13}C$-CH_4 values (Tassi et al., 2012 and references therein), microbial CH_4 usually shows $\delta^{13}C$-CH_4 values <-50 ‰ vs. V-PDB (e.g., Whiticar, 1999), whereas thermogenic CH_4 has been reported to exhibit $\delta^{13}C$-CH_4 values ranging from -50 to -30 ‰ vs. V-PDB. Methane $\delta^{13}C$ from volcanic-hydrothermal systems is usually heavier (Tassi et al., 2012). The sample AN3 plots in Fig. 11 in the field related to the sediment-covered ridge (McCollom and Seewald, 2007) which is intermediate between thermogenic and biogenic fields and consistent with the dominant inputs from microbial methanogenesis and thermal maturation of sedimentary organic matter in the TCCN system. Sample AH1, for which the $\delta^{13}C$-CH_4 value is missing, plots in a line close to the AN3 sample, which might suggest a similar origin for CH_4 and light hydrocarbons as for the Aguas Negras sample.

Aguas Hediondas and Aguas Negras show concentrations of H_2S of 13 and 11 mmol/mol, respectively, which are much higher than e.g. the Chachimbiro geothermal system (Aguilera et al., 2005). Fig. 12 shows the relation between $S/^3He$ ratios and $\delta^{34}S$ values of the TCCN samples, compared to volcanic gases in subduction zones (after Kagoshima et al., 2015). End-member data for the upper mantle, sedimentary pyrite with reduced sulphur derived from the slab, and subducted sulphate are also reported. The $\delta^{34}S$-H_2S values of TCCN samples are positive (+10.67 ‰ and + 6.67 ‰ vs. V-CDT for AH1 and AN3, respectively) and show similar values to most of the arc volcanic-hydrothermal systems (average value +4.6 ‰ vs. V-CDT; Kagoshima et al., 2015). This evidence, coupled with the higher values of $S/^3He$ (AH1: 3.0×10^{10}; AN3: 1.1×10^{10}) compared to the upper mantle end-member (6.5×10^9)

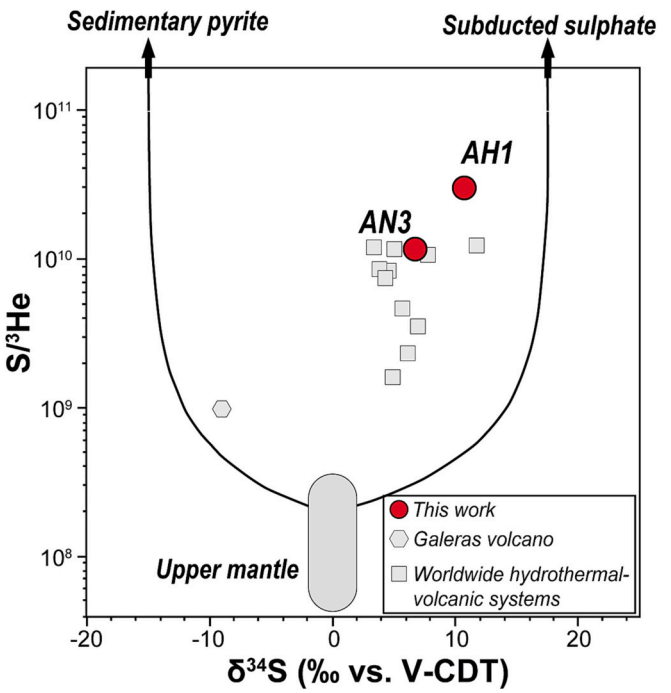

Fig. 12. Correlation diagram between $\delta^{34}S$ (‰ vs. V-CDT) and $S/^3He$ ratios of TCCN gas samples. The S_{tot} and the $\delta^{34}S$ of our samples are related to H_2S. High temperature gas samples from hydrothermal-volcanic circum-Pacific systems are also reported for comparison (Kagoshima et al., 2015). Model endmembers of the upper mantle, sedimentary pyrite and subducted sulphate are included. The curve shows mixing among the end-members. Modified from Kagoshima et al. (2015).

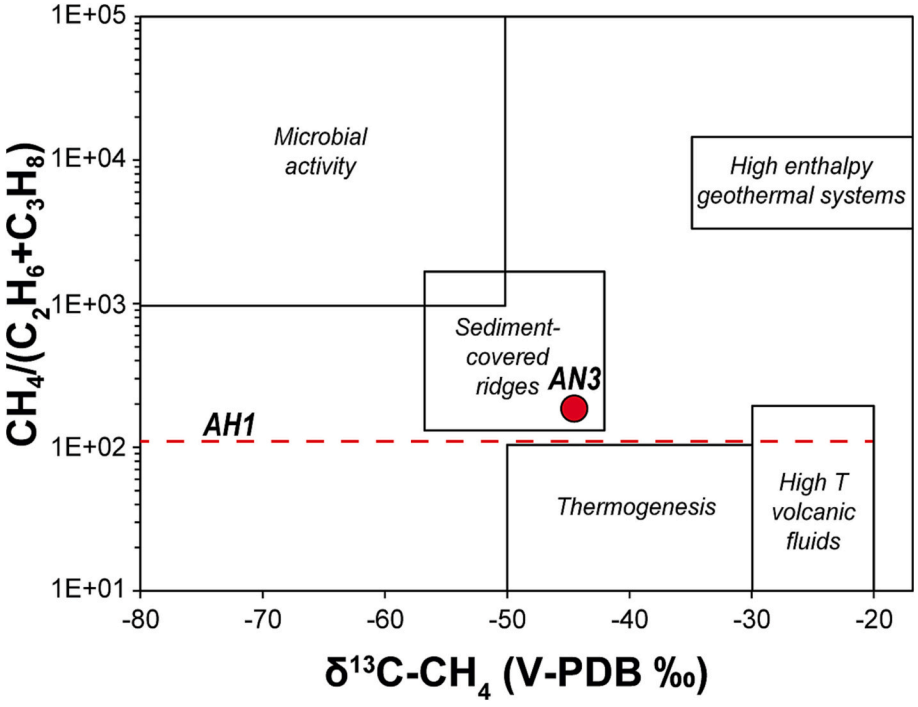

Fig. 11. $\delta^{13}C$-CH_4 (‰ vs. V-PDB) vs. $CH_4/(C_2H_6 + C_3H_8)$ binary plot (from Bernard et al., 1978) for bubbling gases from Aguas Negras thermal spring. Fields of microbial, thermogenic (Whiticar, 1999 and references therein), high-T volcanic fluids, high-enthalpy geothermal systems (Filipovich et al., 2022; Tassi et al., 2012), and sediment covered ridge (McCollom and Seewald, 2007) were also reported. Dashed red line represents the $CH_4/(C_2H_6 + C_3H_8)$ value for AH1 sample (= 133). (For interpretation of the references to color in this figure legend, the reader is referred to the online version of this chapter.)

suggests that the sulphur signature is largely controlled by the incorporation of subducted sulphate (Oppenheimer et al., 2011; Kagoshima et al., 2015) likely in agreement with the $\delta^{34}S$ measured in the sulphate. Noteworthy, the AN3 sample show both $\delta^{34}S$-H_2S and $S/^3He$ values that reveal a higher contribution of upper mantle sulphur with respect to that recognized in Aguas Hediondas.

5.3. Geothermometry

In the TCCN study area, "classical" water geothermometry involving cations compositions (e.g., Na-K-Mg; Giggenbach, 1988) cannot be applied successfully because of the shallow circulation and immaturity of the water samples (Figs. 2 and 4) that are far from reaching an equilibrium with the host rock (Romano and Liotta, 2020).

Gas geothermometry in the H_2O–CO_2–H_2–CO–CH_4 system can be usefully applied to hydrothermal fluids in geothermal exploration (Chiodini and Marini, 1998). In bubbling pools, such as those characterising the fluid discharges in the TCCN area, the H_2O_{vap} concentrations are essentially controlled by water boiling at the surface to a very shallow depth (Tassi et al., 2010). Methane, as previously stated, can be regarded as mainly thermogenic in origin, thus excluding further geothermometric elaborations. Finally, CO concentrations in uprising gases are strongly affected by interactions with shallow aquifers (Shock, 1993; Tassi et al., 2010).

Consequently, a thermodynamic evaluation of gas equilibria in the CO_2–H_2 system was carried out for the TCCN bubbling gases, given its effectiveness in providing information on the thermodynamic conditions dominating at depth (Giggenbach, 1991; Powell, 2000; Sepúlveda et al., 2007). In fact, H_2 is a species that reacts quickly to changes in temperature and redox conditions (Giggenbach, 1987). Hydrogen can be effectively paired with Ar, which is chemically inert and is mostly introduced in the system by the meteoric component (Fig. 7; Giggenbach, 1991), and their molar ratio could be regarded as representative of the deep degassing fluid. This ratio in the liquid phase is controlled by dominating redox conditions. These latter are well represented by the R_H value ($R_H = \log H_2/H_2O$) due to the ability of the H_2/H_2O redox pair to instantaneously adjust in response to variation in redox conditions (Giggenbach, 1980, 1987). The H_2/Ar geothermometer can be coupled with another temperature-sensitive species, i.e., carbon dioxide also normalised to Ar (Giggenbach, 1991).

Considering that in pristine hydrothermal fluids the O_2 is absent (Vaselli et al., 2010), to avoid the effect of possible air atmospheric contamination, Ar values are transformed into Ar*, as follows:

$$Ar^* = Ar–(O_2/22) \quad (1)$$

where the $O_2/22$ ratio is the minimum Ar concentration from air contamination.

The dependence of H_2 on R_H in the liquid phase can be expressed as:

$$Log(H_2/Ar^*) = R_H + 6.52 - log\ (B_{H2}) \quad (2)$$

where B_{H2} is the vapour/liquid distribution coefficient of H_2, whose temperature dependence is given by (Giggenbach, 1980; Fischer and Chiodini, 2015):

$$LogB_{H2} = 6.2283–0.014\ T \quad (3)$$

where T is the temperature in °C.

The dependence of CO_2/Ar* ratios on temperature is given by (Giggenbach, 1991):

$$Log(CO_2/Ar^*) = 0.0277\ T–7.53 + 2048/(T + 273) \quad (4)$$

Graphically, the equilibrium curves for liquid and vapour phases at different R_H values are shown in the $Log(H_2/Ar^*)$ vs. $Log(CO_2/Ar^*)$ diagram (Fig. 13). TCCN gases appear in disequilibrium for the redox conditions related to the FeO/FeO1.5 buffer typical of hydrothermal systems ($R_H = -2.8$; Giggenbach, 1987), plotting below the equilibrium curve at this R_H value (Fig. 13).Our samples appear in a non-equilibrium state also considering redox conditions controlled by the D'Amore and Panichi (1980) redox buffer (DP) that for temperatures between 200 and 250 °C returned values of R_H of −3.45 and − 3.26, respectively. The DP redox buffer has been computed by applying the empirical relationship reported by Sepúlveda et al. (2007):

$$R_{H,EMP} = -1.52 - 911/(T + 273) \quad (5)$$

In Fig. 13, two temperatures of the gases may be read off, an H_2/Ar* temperature (i.e., about 100 °C for both samples), and a CO_2/Ar* temperature (i.e., about 245 and 250 °C for AN3 and AH1, respectively), with the latter possibly representing conditions of the deeper environment (i.e., the geothermal reservoir) (Giggenbach, 1991). These temperatures are higher than those previously reported by INECEL-OLADE-

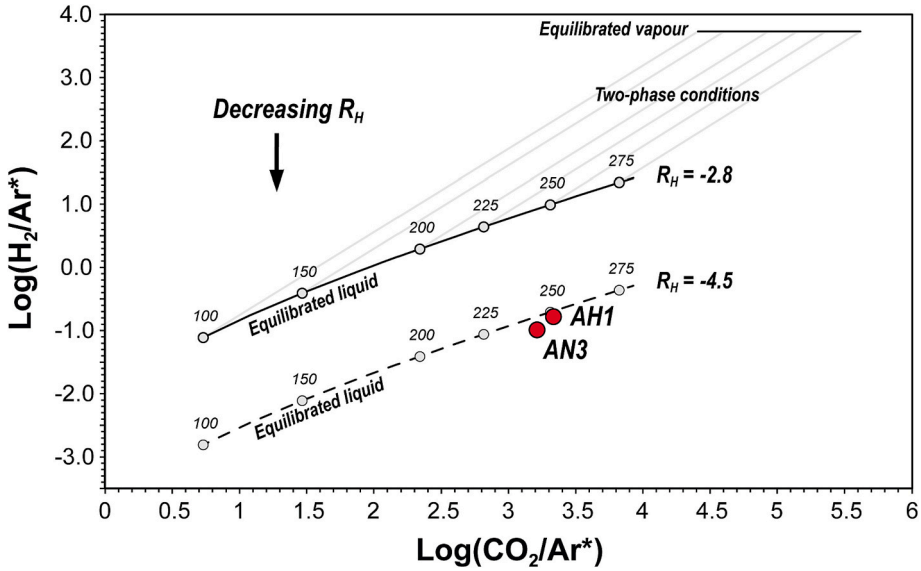

Fig. 13. Binary diagram of $Log(H_2/Ar^*)$ vs. $Log(CO_2/Ar^*)$. The solid lines refer to equilibria in liquid and vapour phases controlled by the FeO/FeO1.5 redox buffer system ($R_H = -2.8$) at temperatures from 100 to 275 °C (Giggenbach, 1987). The dashed line refers to equilibria in a liquid phase based on a more oxidising environment ($R_H = -4.5$).

AQUATER (1987), which computed temperatures of ~220 and ~ 195 °C for Aguas Hediondas and Aguas Negras, respectively.

The apparent disequilibrium of the TCCN gases for the redox conditions related to the FeO/FeO1.5 and DP buffers suggests that these samples represent immature vapours. This could be possibly linked to the input of magmatic-related fluids into the roots of the TCCN geothermal systems which would explain a more negative R_H, thus a more oxidising condition compared to that constrained by the FeO/FeO1.5 buffer, as suggested for other volcanic systems (Chiodini and Marini, 1998; Tassi et al., 2007). In fact, although crustal gases widely affect the TCCN gas composition, the helium and carbon isotopic ratios supported a not negligible mantle contribution to these fluids (Figs. 8, 9, and 12). Moreover, the sampling period (i.e., January 2015) was just after the ending of the seismic crisis that occurred from the end of 2013 until the end of 2014 when the flow of the magmatic fluids into the hydrothermal system should have increased (Ebmeier et al., 2016). Thus, when a more oxidising environment is hypothesized (e.g., R_H ~ −4.5), both samples plot near the equilibrated liquid curve (Fig. 13).

Silica geothermometers (quartz and chalcedony) were also tentatively applied to TCCN samples as they may provide reasonable reservoir temperature estimations also in the non-equilibrium conditions (Joseph et al., 2013 and references therein). Nevertheless, temperatures calculated for equilibria of thermal waters with chalcedony (Arnorsson et al., 1983; Fournier, 1991) and quartz (no steam loss) (Fournier, 1977) show much lower equilibration temperatures with respect to those calculated by using gas phase equilibria, likely due to subsurface mixing with cold water that produces a dilution in the silica concentration. As a matter of fact, gas geothermometry seems to be the only reliable tool to calculate the reservoir temperatures of the TCCN geothermal system.

6. Conceptual model and concluding remarks

Based on the integration of the results of the present study with those of previous investigations (Beate and Urquizo, 2015; Coviello, 2000; Espinoza, 2017), a conceptual model for the TCCN geothermal system is proposed (Fig. 14).

The heat source driving the TCCN geothermal system has been hypothesized as a magmatic body lying at a depth of at least 13 km, as inferred from both magnetotelluric survey (INECEL-OLADE-AQUATER, 1987) and geodetic observations from the unrest episode that occurred in 2014 near Chiles and Cerro Negro volcanoes (Ebmeier et al., 2016). The heat source should feeds a fault-controlled geothermal system consisting of two main layers, located at about 500–1000 m and > 1500 m of depth, respectively, which are topped by a low conductivity level, interpreted as the cap rock (Coviello, 2000). Above these levels, a shallow aquifer is located, mainly consisting of low-salinity waters (e.g., AH2), recharged by meteoric precipitation at altitudes higher than 4100–4200 m as suggested by the δD-H_2O isotopic values (Fig. 2c). The interaction between the shallow aquifer with the geothermal fluids driven to the surface by the tectonic settings produces hypothermal-thermal (T = 20–55 °C), moderately saline, acid Na-(Ca)-SO_4 steam-heated waters which are discharged in the surrounding of the Chiles volcano (AH1, AN3, RB, TRB). At the Aguas Hediondas and Aguas Negras areas, two springs discharged at temperatures higher than 35 °C (AN3) and up to 55 °C (AH1), show strong bubbling due to deep gases reaching the surface. In these springs, likely located in the upflow area of the hydrothermal system, gas geothermometry suggests that the discharged gases are fed by a liquid phase that shows temperatures up to ~245–250 °C, which are some tens degrees higher than those previously estimated (INECEL-OLADE-AQUATER, 1987). The redox conditions indicated by these gases, however, are more oxidising than those typical for geothermal fields (Giggenbach, 1987) and possibly related to the input of magmatic-related fluids into the roots of the TCCN geothermal systems during the volcanic unrest phase that occurred in 2014. Seismic activity occurring at active volcanoes might indeed change the chemical composition of hydrothermal gases (e.g., Ohba et al., 2019; Tedesco and Scarsi, 1999; Vaselli et al., 2010; Vaselli et al., 2019). Unfortunately, the only previous geochemical information on TCCN gases (i.e., Inguaggiato

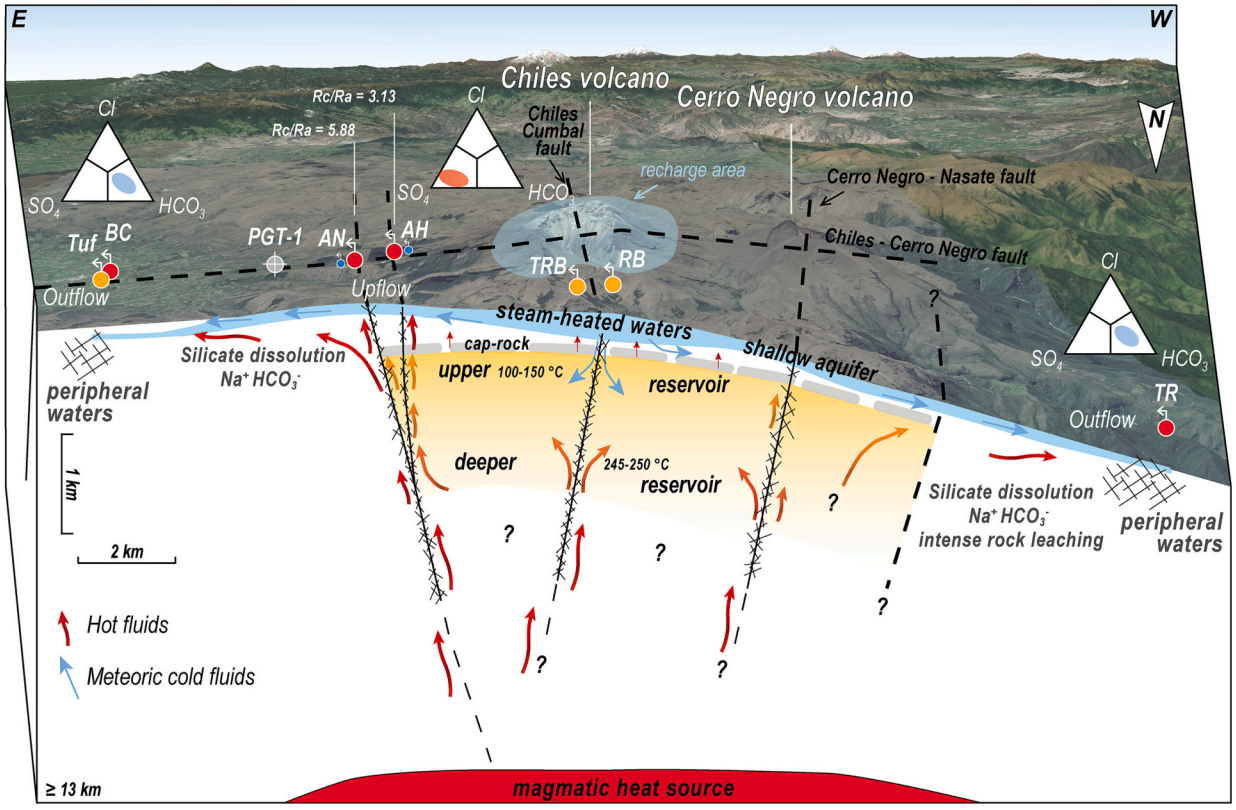

Fig. 14. Conceptual model of the Tufiño-Chiles-Cerro Negro geothermal system in a schematic E-W oriented cross-section (view from the North).

et al., 2010) and the absence of further (i.e., post 2015) data, prevent to make robust assumptions on the specific role played by the seismic activity on the fluid composition. Anyway, mantle contribution is more evident at Aguas Negras when compared to Aguas Hediondas, as emphasized by the sulphur isotopic content of H_2S, and the Rc/Ra, $CO_2/^3He$, and $S/^3He$ ratios, thus suggesting that it could be located at the border of the reservoir where faults approach the heat source and minor interaction with the geothermal reservoir occurs, as observed in other volcanic systems in Southern Andes (e.g., Copahue volcano; Tardani et al., 2021). About 6–7 km far East of the Chiles volcano, thermal and hypothermal waters (Tuf, BC), whose composition is Na-(Mg)-HCO_3, are discharged near the Tufiño village and represent the peripheral waters of the geothermal system. On the other side, about 7 km NW of Cerro Negro volcano, the Termal del Rio (TR sample) shows similar temperature (33 °C) and chemical composition of the Tufiño's waters, but higher TDS and long-term circulation characteristics, also related to the addition of possible Boron-bearing vapours, suggesting that the hydrothermal system could extend to the west of the Chiles volcano as well.

Waters analysed in this work are generally immature, deriving from the interaction and mixing between deep-hot and shallow-cold fluids. However, at El Hondón spring, located about 6 km SSE of Chiles volcano (Fig. 1) - and apparently on the same N-S trending tectonic structure of AH and AN - near-neutral (pH = 7.1 and 7.7), salty (EC = 5766 and 6340 μs/cm) and hot (T = 85.1 and 85.8 °C) fluids are discharged, which might reveal the presence of brines associated with the geothermal reservoir. Analytical data on El Hondón, as well as on several other springs to the W and SE of Chiles Volcano (Fig. 1; analysis not available in the literature), are therefore needed to shed light on this hypothesis and further improve the conceptual model of the Tufiño-Chiles-Cerro Negro geothermal system. Monitoring of fluids' main parameters through time would also be of paramount interest to deepen the complex interactions among the volcano-tectonic seismicity driven by fluid-pressure changes (i.e., 2013–2014 seismic swarms), the magmatic vs. hydrothermal fluids and the peripheral waters circulation.

CRediT authorship contribution statement

Marco Taussi: Conceptualization, Methodology, Visualization, Data curation, Validation, Investigation, Writing - original draft, Writing - review & editing, Supervision.

Daniele Tardani: Validation, Methodology, Data curation, Investigation, Writing - original draft, Writing - review & editing.

Franco Tassi: Methodology, Investigation, Validation, Supervision, Writing - review & editing.

Andrea Gorini: Data acquisition, Writing - review & editing.

Eduardo Aguilera: Writing - review & editing.

Bruno Capaccioni: Resources, Data acquisition, Methodology, Investigation.

Alberto Renzulli: Resources, Data acquisition, Funding acquisition, Project administration, Writing - review & editing.

Declaration of competing interest

The authors declare that they have no known competing financial interests or personal relationships that could have appeared to influence the work reported in this paper.

Data availability

The data supporting the findings of this study are available within the article.

Acknowledgements

Our thoughts turn to our beloved colleague and friend Bruno Capaccioni who led the sampling activity of waters and gas at TCCN during January 2015, and tragically passed away in September 2016. We are also grateful to Mauro Ferraris, an explorer, climber, and geologist having a great knowledge on the Ecuadorian volcanoes, who organized the logistics of the fluid geochemistry campaign in Ecuador. This work was part of the PhD project of A. Gorini and financially supported by the University of Urbino and University of Florence. We are grateful to the anonymous Reviewer and the Associate Editor for their valuable comments. The Editor-in-Chief is also thanked for editorial handling.

References

Aguilera, E., Cioni, R., Gherardi, F., Magro, G., Marini, L., Zhonghe, P., 2005. Chemical and isotope characteristics of the Chachimbiro geothermal fluids (Ecuador). Geothermics 34, 495–517.

Alfaro, C., Rodriguez, G., 2021. Status of the Geothermal Resouces of Colombia: Country Update. Proceedings World Geothermal Congress 2020+1, Reykjavik, Iceland, April-October 2021.

Alfaro, C., Rueda-Gutiérrez, J.B., Casallas, Y., Rodríguez, G., Malo, J., 2021. Approach to the geothermal potential of Colombia. Geothermics 96, 102169.

Almeida, E., 1990. Alternativas para el desarrollo geotermoeléctrico en la República del Ecuador. Unp. Tech. Report for INECEL.

Almeida, E., Sandoval, G., Panichi, C., Noto, P., Bellucci, L., 1992. Modelo geotermico preliminar de areas volcanicas del Ecuador, a partir de estudios químicos e isotópicos de manifestaciones termales. In: Proceedings of the Meeting "Geothermal Investigations With Isotope and Geochemical Techniques in Latin America" Held in San José, Costa Rica, 12-16 November 1990.

Ancellin, M.A., Samaniego, P., Vlastélic, I., Nauret, F., Gannoun, A., Hidalgo, S., 2017. Across-arc versus along-arc Sr-Nd-Pb isotope variations in the Ecuadorian volcanic arc. Geochem. Geophys. Geosyst. 18 https://doi.org/10.1002/2016GC006679.

Arnorsson, S., Gunnlaugsson, E., Svavarsson, H., 1983. The chemistry of geothermal waters in Iceland. III. Chemical geothermometry in geothermal investigations. Geochim. Cosmochim. Acta 47 (3), 567–577.

Barckhausen, U., Ranero, C.R., Cande, S.C., Engels, M., Weinrebe, W., 2008. Birth of an intraoceanic spreading center. Geology 36, 767.

Barry, P.H., De Moor, J.M., Chiodi, A., Aguilera, F., Hudak, M.R., Bekaert, D.V., Turner, S.J., Curtice, J., Seltzer, A.M., Jessen, G.L., Osses, E., Blamey, J.M., Amenábar, M.J., Selci, M., Cascone, M., Bastianoni, A., Nakagawa, M., Filipovich, R., Bustos, E., Schrenk, M.O., Buongiorno, J., Ramírez, C.J., Rogers, T.J., Lloyd, K.G., Giovannelli, D., 2022. The helium and carbon isotope characteristics of the Andean convergent margin. Front. Earth Sci. 10, 897267 https://doi.org/10.3389/feart.2022.897267.

Beate, B., Urquizo, M., 2015. Geothermal Country Update for Ecuador: 2010 – 2015. Proceedings World Geothermal Congress 2015, Melbourne, Australia, 19-25 April.

Beate, B., Urquizo, M., Loret, A., 2021. Geothermal Country Update for Ecuador: 2015 – 2020. Proceedings World Geothermal Congress 2020+1, Reykjavik, Iceland, April-October 2021.

Bernard, B.B., Brooks, J.M., Sackett, W.M., 1978. A geochemical model for characterization of hydrocarbon gas sources in marine sediments. In: Offshore Technology Conference, Houston, USA, pp. 435–438.

Bocanegra, L.C., Sánchez, J.J., 2017. Mapa de fallas de los volcanes Chiles-Cerro Negro (Nariño) a partir de minería de datos y confirmación de campo. Bol. Geol. 39 (3), 71–86.

Bona, P., Coviello, M., 2016. Valoración y gobernanza de los proyectos geotérmicos en América del Sur: una propuesta metodológica.. In: Comisión Económica para América Latina y el Caribe (CEPAL), United Nations, p. 178.

Bryant, J.A., Yogodzinski, G.M., Hall, M.L., Lewicki, J.L., Bailey, D.G., 2006. Geochemical constraints on the origin of volcanic rocks from the andean Northern volcanic zone, Ecuador. J. Petrol. 47 (6), 1147–1175. https://doi.org/10.1093/petrology/egl006.

Capaccioni, B., Tassi, F., Renzulli, A., Vaselli, O., Menichetti, M., Inguaggiato, S., 2014. Geochemistry of thermal fluids in NW Honduras: new perspectives for exploitation of geothermal areas in the southern Sula graben. J. Volcanol. Geotherm. Res. 280, 40–52.

Carrera, V.D.V., Guevare, G.P.V., 2016. Fuentes termales del Ecuador. Universidad de las Fuerzas Armadas ESPE, Sangolquí, Ecuador. www.espe.edu.ec.

Celec-Isagen, 2015. In: Informe geológico parcial del proyecto geotérmico binacional Tufiño-Chiles-Cerro Negro. Informe técnico inédito del SYR, para Celec-Isagen, p. 144.

Cepeda, H., Acevedo, A.P., Lesmes, L.E., 1987. Características químicas y petrográficas de los volcanoes Azufral, Cumbal y Chiles-Cerro Negro, Colombia, S.A. Informe. Ingeominas, 25 pp. Medellín.

Chiodini, G., Marini, L., 1998. Hydrothermal gas equilibria: the H2O-H2-CO2-CO-CH4 system. Geochim. Cosmochim. Acta 62 (15), 2673–2687.

Cortés, G., Calvache, M., 1996. In: Investigación sobre la evolución y composición de los volcanes de Colombia: Galeras y Volcanes del Sur. Geología de los Volcanes Chiles y Cerro Negro. Informe Interno. INGEOMINAS, p. 53.

Coviello, M., 2000. Estudio para la Evaluación del Entorno del Proyecto Geotérmico Binacional "Tufiño-Chiles-Cerro Negro". In: Proyecto OLADE/CEPAL/GTZ, p. 79. http://www.cepal.org/publicaciones/xml/6/5696/LCR1995-E.pdf.

Craig, H., 1961. Isotopic variations in meteoric waters. Science 133 (3465), 1702–1703.

D'Amore, F., Panichi, C., 1980. Evaluation of deep temperatures of hydrothermal systems by a new gas geothermometer. Geochim. Cosmochim. Acta 44, 549–556.
Droux, A., Delaloye, M., 1996. Petrography and geochemistry of Plio-Quaternary Calc-Alkaline volcanoes of Southwestern Colombia. J. S. Am. Earth Sci. 9 (1/2), 27–41.
Ebmeier, S.K., Elliott, J.R., Nocquet, J.-M., Biggs, J., Mothes, P., Jarrín, P., Yépez, M., Aguaiza, S., Lundgren, P., Samsonov, S.V., 2016. Shallow earthquake inhibits unrest near Chiles-Cerro Negro volcanoes, Ecuador-colombian border. Earth Planet. Sci. Lett. 450, 283–291.
Ellis, A.J., Mahon, W.A.J., 1977. In: Chemistry and Geothermal Systems. Academic Press, New York, pp. 1–392.
Espinoza, C.C.G., 2017. In: Caracterización de la secuencia litoestratigráfica y de la mineralogía de alteración hidrotermal del pozo PGT-1 del proyecto geotérmico Tufiño-Chiles, provincia del Carchi. Escuela Politecnica Nacional, Quito, Ecuador, p. 182. Master thesis (in spanish).
Filipovich, R., Chiodi, A., Baez, W., Ahumada, M.F., Invernizzi, C., Taviani, S., Aldega, L., Tassi, F., Barrios, A., Corrado, S., Groppelli, G., Norini, G., Bigi, S., Caricchi, C., De Benedetti, A., De Astis, G., Becchio, R., Viramonte, J.G., Giordano, G., 2022. Structural analysis and fluid geochemistry as tools to assess the potential of the Tocomar geothermal system, Central Puna (Argentina). Geothermics 98, 102297.
Fischer, T.P., Chiodini, G., 2015. Volcanic, Magmatic and Hydrothermal Gases. The Encyclopedia of Volcanoes. Elsevier. https://doi.org/10.1016/B978-0-12-385938-9.00045-6.
Fischer, T.P., Sturchio, N.C., Stix, J., Arehart, G.B., Counce, D., Williams, S.N., 1997. The chemical and isotopic composition of fumarolic gases and spring discharges from Galeras Volcano, Colombia. J. Volcanol. Geotherm. Res. 77, 229–253.
Fouillac, C., Michard, G., 1981. Sodium/ lithium ratio in water applied to geothermometry of geothermal reservoirs. Geothermics 10, 55–70.
Fournier, R.O., 1977. Chemical geothermometers and mixing models for geothermal systems. Geothermics 5 (1–4), 41–50.
Fournier, R.O., 1991. Water geothermometers applied to geothermal energy. In: D'Amore, Franco (Ed.), Application of Geochemistry in Geothermal Reservoir Development. Unitar/UNDP, pp. 37–69.
Garcia, Y.K., Sanchez, J.J., 2019. Contribuciones geológicas al Modelo conceptual geotérmico en la región de los volcanes Chiles – Cerro Negro (Colombia-Ecuador). Bol. Geol. 41 (1), 151–171. https://doi.org/10.18273/revbol.v41n1-2019008.
Gawell, K., Reed, M., Wright, M., 1999. Preliminary Report: Geothermal Energy, the Potential for Clean Power from the Earth. Geothermal Energy Association Report. April, 1999.
Giggenbach, W.F., 1980. Geothermal gas equilibria. Geochim. Cosmochim. Acta 44 (12), 2021–2032.
Giggenbach, W.F., 1987. Redox processes governing the chemistry of fumarolic gas discharges from White Island, New Zealand. Appl. Geochem. 2 (2), 143–161.
Giggenbach, W.F., 1988. Geothermal solute equilibria. Derivation of Na-K-Mg-Ca geoindicators. Geochim. Cosmochim. Acta 52, 2749–2765.
Giggenbach, W.F., 1991. Chemical techniques in geothermal exploration. In: D'Amore, Franco (Ed.), Application of Geochemistry in Geothermal Reservoir Development. Unitar/UNDP, pp. 119–144.
Giggenbach, W.F., 1995. Variations in the chemical and isotopic composition of fluids discharged from the Taupo Volcanic Zone, New Zealand. J. Volcanol. Geotherm. Res. 68, 89–116.
Giggenbach, W.F., Goguel, R.L., 1989. Collection and Analysis of Geothermal and Volcanic Water and Gas Discharges. DSIR Chemistry, Report 2401.
Giggenbach, W.F., Sano, Y., Wakita, H., 1993. Isotopic composition of helium, and CO2 and CH4 contents in gases produced along the New Zealand part of a convergent plate boundary. Geochim. Cosmochim. Acta 57, 3427–3455.
Gómez, Diaz E., Marín Cerón, M.I., 2020. Hydrogeochemical characteristics at Doña Juana complex (SW Colombia): a new area for geothermal exploration in the Northern Andes region. Geothermics 84, 101738.
Gutscher, M.A., Malavieille, J., Lallemand, S., Collot, J.Y., 1999. Tectonic segmentation of the North andean margin: impact of the Carnegie Ridge collision. Earth Planet. Sci. Lett. 168, 255–270.
Hall, M.L., Beate, B., 1991. El volcanismo Plio-Cuaternario en los Andes del Ecuador. Estud. Geographicos 4, 5–38.
Hall, M.L., Samaniego, P., Le Pennec, J.-L., Johnson, J.B., 2008. Ecuadorian Andes volcanism: a review of late Pliocene to present activity. J. Volcanol. Geotherm. Res. 176 (1), 1–6.
Hidalgo, S., Gerbe, M.C., Martin, H., Samaniego, P., Bourdon, E., 2012. Role of crustal and slab components in the Northern Volcanic Zone of the Andes (Ecuador) constrained by Sr–Nd–O isotopes. Lithos 132–133, 180–192.
Hilton, D.R., McMurtry, G.M., Goff, F., 1998. Large variations in vent fluid CO2/3He ratios signal rapid changes in magma chemistry at Loihi Seamount, Hawaii. Nature 396, 359–362.
Hilton, D.R., Fischer, T.P., Marty, B., 2002. Noble gases and Volatile Recycling at Subduction zones. Rev. Mineral. Geochem. 47 (1), 319–370.
Hoefs, J., 2009. Stable Isotope Geochemistry. Springer, Berlin, Heidelberg. https://doi.org/10.1007/978-3-540-70708-0, 286 pp.
ICEL, 1983. Proyecto geotérmico Chiles-Cerro Negro. Fase I etapa de prefactibilidad. Informe preliminar, Bogotá, 146 pp.
IG-EPN, 2014. Instituto Geofísico Escuela Nacional Politecnica, Informe del volcán Chiles–Cerro Negro n.27, November 2014.
IG-EPN, 2019a. Instituto Geofísico Escuela Nacional Politecnica, Informe de visita a las fuentes termales y campos fumarólicos asociados al complejo volcánico Chiles–Cerro Negro, November 2019.
IG-EPN, 2019b. Instituto Geofísico Escuela Nacional Politecnica, Informe especial complejo volcánico Chiles–Cerro Negro n.1, August 2019.
IG-EPN, 2019c. Instituto Geofísico Escuela Nacional Politecnica, Informe del volcán Chiles–Cerro Negro: Reporte de los trabajos efectuados en el complejo volcánico Chiles - Cerro Negro (multigas, parámetros físico - químicos), January 2020, 286 pp.
INECEL-OLADE-AQUATER, 1987. Proyecto Geotermico Binacional Tufiño-Chiles-Cerro Negro, informe de prefactibilidad, modelo geotérmico síntesis y recomendaciones. Unp. Tech. Report.
Inguaggiato, S., Rizzo, A., 2004. Dissolved helium isotope ratios in ground-waters: a new technique based on gas–water reequilibration and its application to a volcanic area. Appl. Geochem. 19, 665–673.
Inguaggiato, S., Hidalgo, S., Beate, B., Bourquin, J., 2010. Geochemical and Isotopic characterization of Volcanic and Geothermal Fluids discharged from the Ecuadorean Volcanic Arc. Geofluids 10–4, 525–541.
Joseph, E.P., Fournier, N., Lindsay, J.M., Robertson, R., Beckles, D.M., 2013. Chemical and isotopic characteristics of geothermal fluids from Sulphur Springs, Saint Lucia. J. Volcanol. Geotherm. Res. 254, 23–36.
Kagoshima, T., Sano, Y., Takahata, N., Maruoka, T., Fischer, T.P., Hattori, K., 2015. Sulphur geodynamic cycle. Sci. Rep. 5, 8330.
Koch, C.D., Delph, J., Beck, S.L., Lynner, C., Ruiz, M., Hernandez, S., Samaniego, P., Meltzer, A., Mothes, P., Hidalgo, S., 2021. Crustal thickness and magma storage beneath the Ecuadorian arc. J. S. Am. Earth Sci. 110, 103331.
Lages, J., Rizzo, A.L., Aiuppa, A., Samaniego, P., Le Pennec, J.L., Ceballos, P., Narvaez, P. A., Moussallam, Y., Bani, P., Ian, Schipper C., Hidalgo, S., Gaglio, V., Alberti, E., Sandoval-Velasquez, A., 2021. Noble gas magmatic signature of the andean Northern Volcanic Zone from fluid inclusions in minerals. Chem. Geol. 559, 119966.
Lesmes, L.E., Bobadilla, L., Hernández, M.L., Cañón, Y., Mojica, J., Garzón, G., 2004. Mineralogía y fisicoquímica de las Fuentes termales del departamento de Nariño. Bol. Geol. 26 (42), 57–66.
Lewicki, J.L., Fischer, T.P., Williams, S.N., 2000. Chemical and isotopic compositions of fluids at Cumbal Volcano, Colombia: evidence for magmatic contribution. Bull. Volcanol. 62, 347–361.
Mamyrin, B.A., Tolstikhin, I.N., 1984. Helium Isotopes in Nature. Elsevier, Amsterdam, 273 pp.
Marini, L., Moretti, R., Accornero, M., 2011. Sulfur isotopes in magmatic-hydrothermal systems, melts, and magmas. Rev. Mineral. Geochem. 73, 423–492.
Maza, S.N., Collo, G., Morata, D., Taussi, M., Vidal, J., Mattioli, M., Renzulli, A., 2021. Active and fossil hydrothermal zones of the Apacheta volcano: insights for the Cerro Pabellón hidden geothermal system (Northern Chile). Geothermics 96, 102206.
McCollom, T.M., Seewald, J.S., 2007. Abiotic synthesis of organic compounds in deep-sea hydrothermal environments. Chem. Rev. 107, 382–401.
Mejía, E., Rayo, L., Méndez, J., Echeverri, J., 2014. Geothermal Development in Colombia. Proceedings of "Short Course VI on Utilization of Low- and Medium-Enthalpy Geothermal Resources and Financial Aspects of Utilization", Organized by UNU-GTP and LaGeo, in Santa Tecla, El Salvador, March 23-29, 2014.
Michaud, F., Chabert, A., Collot, J.-Y., Sallarès, V., Flueh, E.R., Charvis, P., Graindorge, D., Gutscher, M.-A., Bialas, G., 2005. Fields of multikilometer-scale sub-circular depressions in the Carnegie Ridge sedimentary blanket: effect of underwater carbonate dissolution? Mar. Geol. 216, 205–219.
Michaud, F., Witt, C., Royer, J.-Y., 2009. Influence of the subduction of the Carnegie volcanic ridge on Ecuadorian geology: reality and fiction. Geol. Soc. Am. Mem. 204 (10), 217–228.
Mix, A.C., Tiedemann, R., Blum, P., Leg 202 Shipboard Scientific Party, 2003. Proceedings of the Ocean Drilling Program (ODP) Initial Reports, Volume 202: College Station, Texas, Ocean Drilling Program, 145 pp.
Monsalve, B.M.L., 2020. The volcanic front in Colombia: segmentation and recent and historical activity. In: Gómez, J., Pinilla–Pachon, A.O. (Eds.), The Geology of Colombia, Volume 4 Quaternary, 38. Servicio Geológico Colombiano, Publicaciones Geológicas Especiales, Bogotá, pp. 97–159. https://doi.org/10.32685/pub.esp.38.2019.03.
Monsalve, B.M.L., Laverde, C.C.A., 2016. Contribución al Registro histórico de actividad de los Volcanes Chiles y Cerro Negro (frontera Colombo-ecuatoriana). Bol. Geol. 38 (4), 61–78.
Montegrossi, G., Tassi, F., Vaselli, O., Buccianti, A., Garofalo, K., 2001. Sulphur species in volcanic gases. Anal. Chem. 73 (15), 3709–3715.
Müller, R.D., Sdrolias, M., Gaina, C., Roest, W.R., 2008. Age, spreading rates and spreading asymmetry of the world's ocean crust. Geochem. Geophys. Geosyst. 9 (4), 1–19.
Nisi, B., Vaselli, O., Tassi, F., Elio, J., Ortega, M., Caballero, J., Rappuoli, D., Mazadiego, L.F., 2013. Origin of the gases released from the Acqua Passante and Ermeta wells (Mt. Amiata, central Italy) and possible environmental implications for their closure. Ann. Geophys. 57 (4), S0438 https://doi.org/10.4401/ag-6584, 146 pp.
Ohba, T., Yaguchi, M., Nishino, K., Numanami, N., Daita, Y., Sukigara, C., Ito, M., Tsunogai, U., 2019. Time variations in the chemical and isotopic composition of fumarolic gases at Hakone volcano, Honshu Island, Japan, over the earthquake swarm and eruption in 2015, interpreted by magma sealing model. Earth Planets Space 71, 48.
Oppenheimer, C., Scaillet, B., Martin, R.S., 2011. In: Sulfur Degassing From Volcanoes: Source Conditions, Surveillance, Plume Chemistry and Earth System Impacts. Reviews in Mineralogy and Geochemistry, Mineralogical Society, 73, pp. 363–421.
Poreda, R.J., Jeffrey, A.W.A., Kaplan, L.R., Craig, H., 1988. Magmatic helium in subduction-zone natural gases. Chem. Geol. 71, 199–210.
Powell, T., 2000. A review of exploration gas geothermometry. In: Proceedings, Twenty-Fifth Workshop on Geothermal Reservoir Engineering Stanford University, Stanford, California, January 24-26, 2000.
Romano, P., Liotta, M., 2020. Using and abusing Giggenbach ternary Na-K-Mg diagram. Chem. Geol. 541, 119577.

Ruiz, M., 2015. Temporal Evolution of a Seismic Swarm at Chiles-Cerro Negro Volcanic Complex. European Geosciences Union, General Assembly 2015, Vienna.
Salazar, S.S., Muñoz, Y., Ospino, A., 2017. Analysis of geothermal energy as an alternative source for electricity in Colombia. Geotherm. Energy 5 (27), 1–12.
Sano, Y., Marty, B., 1995. Origin of carbon in fumarolic gases from island arcs. Chem. Geol. 119, 265–274.
Sano, Y., Williams, S.N., 1996. Fluxes of mantle and subducted carbon along convergent plate boundaries. Geophys. Res. Lett. 23, 2749–2752.
Sano, Y., Gamo, T., Williams, S.N., 1997. Secular variations of helium and carbon isotopes at Galeras volcano, Colombia. J. Volcanol. Geotherm. Res. 77, 255–265.
Sano, Y., Nishio, Y., Sasaki, S., Gamo, T., Nagao, K., 1998. Helium and carbon isotope systematics at Ontake volcano, Japan. J. Geophys. Res. 103 (B10), 23863–23873.
Santamaria, S., Telenchana, E., Benjamin, B., Hidalgo, S., Beate, B., Cordova, M., Narvaez, D., 2017. Registro de erupciones ocurridas en los Andes del Norte durante el Holoceno: Nuevos resultados obtenidos en la turbera de Potrerillos, Complejo Volcánico Chiles-Cerro Negro. Rev. Politécnica 39 (2), 7–15.
Schoell, M., 1980. The hydrogen and carbon isotopic composition of methane from natural gases of various origins. Geochim. Cosmochim. Acta 44, 649–661.
Sepúlveda, F., Lahsen, A., Powell, T., 2007. Gas geochemistry of the Cordón Caulle geothermal system, Southern Chile. Geothermics 36 (5), 389–420.
Seton, M., Mueller, R.D., Zahirovic, S., Gaina, C., Torsvik, T., Shepard, G., Talsma, A., Gurnis, M., Turner, M., Chandler, M., 2012. Global continental and ocean basin reconstructions since 200 Ma. Earth Sci. Rev. 113, 212–270.
SGC, 2020. Base de datos de Inventario Nacional de Manifestaciones Hidrotermales de Colombia Grupo Exploración de Recursos Geotérmicos, Servicio Geológico Colombiano (2020). http://hidrotermales.sgc.gov.co/invtermales/.
Shaw, A.M., Hilton, D.R., Fischer, T.P., Walker, J.A., Alvarado, G., 2003. Contrasting volatile systematics of Nicaragua and Costa Rica: insights to C-cycling through subduction zones. Earth Planet. Sci. Lett. 214 (3–4), 499–513.
Shock, E.L., 1993. Hydrothermal dehydration of aqueous organic compounds. Geochim. Cosmochim. Acta 57, 3341–3349.
Snyder, G., Poreda, R., Fehn, U., Hunt, A., 2003. Sources of nitrogen and methane in Central American geothermal settings: noble gas and 129I evidence for crustal and magmatic volatile components. Geochem. Geophys. Geosyst. 4.
Stern, C.R., 2004. Active Andean volcanism: its geologic and tectonic setting. Rev. Geol. Chile 31 (2), 161–206.
Taborda, A., Portela, J.P., Lopez-Sanchez, J., Daniele, L., Moreno, D., Blessent, D., 2022. Temperature estimation of the Nevado del Ruiz Volcano geothermal reservoir: insights from western hot springs hydrogeochemistry. J. Geochem. Explor. 240, 107049.
Tardani, D., Reich, M., Roulleau, E., Takahata, N., Sano, Y., Pérez Flores, P., Sanchez-Alfaro, P., Cembrano, J., Arancibia, G., 2016. Exploring the structural controls on helium, nitrogen and carbon isotope signatures in hydrothermal fluids along an intra-arc fault system. Geochim. Cosmochim. Acta 184, 193–211.
Tardani, D., Roulleau, E., Pinti, D.L., Pérez-Flores, P., Daniele, L., Reich, M., Sanchez-Alfaro, P., Morata, D., Richard, L., 2021. Structural control on shallow hydrogeochemical processes at Caviahue-Copahue Volcanic complex (CCVC), Argentina. J. Volcanol. Geotherm. Res. 414, 107228.
Tassi, F., Vaselli, O., Capaccioni, B., Montegrossi, G., Barahona, F., Caprai, A., 2007. Scrubbing processes and chemical equilibria controlling the composition of light hydrocarbons in natural gas discharges: an example from the geothermal fields of Salvador. Geochem. Geophys. Geosyst. 8, Q05008.
Tassi, F., Aguilera, F., Darrah, T., Vaselli, O., Capaccioni, B., Poreda, R.J., Delagado-Huertas, A., 2010. Fluid geochemistry of hydrothermal systems in the Arica-Parinacota, Tarapaca and Antofagasta regions (northern Chile). J. Volcanol. Geotherm. Res. 192 (1–2), 1–15.
Tassi, F., Fiebig, J., Vaselli, O., Nocentini, M., 2012. Origins of methane discharging from volcanic-hydrothermal, geothermal and cold emissions in Italy. Chem. Geol. 310, 36–48.
Tedesco, D., Scarsi, P., 1999. Chemical (He, H2, CH4, Ne, Ar, N2) and isotopic (He, Ne, Ar, C) variations at the solfatara crater (southern italy): mixing of different sources in relation to seismic activity. Earth Planet. Sci. Lett. 171 (3), 465–480.
Vaselli, O., Tassi, F., Montegrossi, G., Capaccioni, B., Giannini, L., 2006. Sampling and analysis of volcanic gases. Acta Volcanol. 18, 65–76.
Vaselli, O., Tassi, F., Duarte, E., Fernandez, E., Poreda, R.J., Delagado-Huertas, A., 2010. Evolution of fluid geochemistry at the Turrialba volcano (Costa Rica) from 1998 to 2008. Bull. Volcanol. 72, 397–410.
Vaselli, O., Tassi, F., Fischer, T.P., Tardani, D., Fernández, E., del Mar Martínez, M., de Moor, M.J., Bini, G., 2019. The last eighteen years (1998–2014) of fumarolic degassing at the poás Volcano (Costa Rica) and renewal activity. In: Tassi, F., Vaselli, O., Mora-Amador, R.A. (Eds.), Poás Volcano: The Pulsing Heart of Central America Volcanic Zone, 2019. Springer International Publishing, Switzerland, pp. 235–260.
Vélez, M.I., Blessent, D., Cordoba, S., Lopez-Sanchez, J., Raymond, J., Parra-Palacio, E., 2018. Geothermal potential assessment of the Nevado del Ruiz volcano based on rock thermal conductivity measurements and numerical modeling of heat transfer. J. S. Am. Earth Sci. 81, 153–164.
Whiticar, M.J., 1999. Carbon and hydrogen isotope systematics of bacterial formation and oxidation of methane. Chem. Geol. 161, 291–314.